1	Extratropical forcing of low-latitude subsurface oxygenation under future
2	warming
3	Zhen Gao <sup>1,2</sup> , Shantong Sun <sup>2,1*</sup> , Daoxun Sun <sup>2</sup> , Jimin Yu <sup>2</sup> , and Lixin Wu <sup>2</sup>
4	<sup>1</sup> College of Oceanic and Atmospheric Science, Ocean University of China, Qingdao, China
5	<sup>2</sup> Laoshan Laboratory, Qingdao, China
6	Corresponding author: Shantong Sun ( <u>stsun@qnlm.ac</u> )
7	
8	
9	This manuscript is a non-peer reviewed preprint submitted to EarthArXiv, and has
10	also been submitted to Science Advances for peer review.
11	
12	
13	
14	
15	
16	
17	
18	
19	
20	
21	
22	
23	
24	
25	
26	
27	
28	
29	
30	

#### **Abstract**

The global ocean is losing oxygen under climate warming, yet most climate models project rising oxygen levels in low-latitude subsurface waters (~100–500 m), partly due to their enhanced ventilation. However, underlying drivers for the enhanced ventilation remain unclear. Here we demonstrate that the enhanced tropical subsurface ventilation is driven by extratropical forcing. While extratropical warming/freshening are typically associated with weakened subsurface ventilation in the subtropics due to reduced subduction of mode and intermediate waters, they also induce cross-hemispheric overturning responses that deepen isopycnals and thereby effectively push well-ventilated, oxygen-rich shallower waters to greater depths, which improves ventilation and increases oxygen in tropical subsurface waters. These processes can reduce the deoxygenation stress in tropical subsurface depths on centennial timescales, but their effects diminish on longer time scales. Our findings highlight critical links between extratropical dynamics and tropical subsurface oxygen fluctuations, with critical implications for projecting climatic impacts on marine ecosystems.

#### Introduction

The global ocean is losing oxygen due to rising temperatures (Keeling et al., 2010; Helm et al., 2011; Ito et al., 2017; Schmidtko et al., 2017), potentially affecting the ocean nutrient cycle with adverse impacts on marine ecosystems (Vaquer-Sunyer and Duarte, 2008; Stramma et al., 2011). This deoxygenation trend is expected to continue over the 21<sup>st</sup> century as warming decreases oxygen solubility in seawater and surface ocean stratification enhancement reduces the oxygen supply to the ocean interior (Oschlies et al., 2018; Keeling and Garcia, 2002; Bopp et al., 2002, 2017). However, in contrast to the global deoxygenation trend, most climate models project an oxygen increase in the tropical subsurface ocean (Fig. 1a; Bopp et al., 2013; Kwiatkowski et al., 2020; Busecke et al., 2022), currently hosting the ocean's oxygen minimum zones. This oxygen gain may potentially lead to a contraction of oxygen minimum zones (Busecke et al., 2022), reducing oceanic production of nitrous oxide (Babbin et al., 2015) — a potent greenhouse gas — and thereby creating a negative feedback to counteract

climate warming.

61

62

63

64

65

66

67

68

69

70

71

72

73

74

75

76

77

78

79

80

81

82

83

84

85

86

87

88

89

90

Both biological and physical changes have been invoked to explain the projected tropical subsurface oxygen gain (Bopp et al., 2017; Takano et al., 2018; Ditkovsky and Resplandy, 2025). As the climate warms, the upper-ocean stratification strengthens and the global ocean overturning circulation weakens (Capotondi et al., 2012; Li et al., 2020; Bakker et al., 2016; Weijer et al., 2020), both reducing nutrients in the upper ocean (Keeling and Garcia, 2002; Moore et al., 2018; Kwiatkowski et al., 2020; Sun et al., 2024). The nutrient decline weakens biological productivity, reducing organic matter export and thereby decreasing subsurface oxygen consumption (Bopp et al., 2002). The warming climate also drives global ventilation changes (Fig. 1b), with enhanced ventilation in the tropical subsurface that contributes to the oxygen gain (Gnanadesikan et al., 2007, 2012; Takano et al., 2018; Ditkovsky and Resplandy, 2025). A quantitative attribution of the tropical subsurface oxygen gain to biological vs. ventilation changes is model-dependent, given the large uncertainty in representing biological activities in models (e.g., Séférian et al., 2020; Rohr et al., 2023). As such, we will focus on physical processes responsible for the ventilation changes in this study. The improved ventilation in the tropical subsurface, largely occurring within the thermocline's "shadow zones" (Luyten et al., 1983), contrasts with projections of reduced subduction of mode waters under climate warming (Downes et al., 2009; Luo et al., 2009; Xu et al., 2012). This counterintuitive ventilation improvement in the tropical subsurface has been primarily linked to increased local stratification, which may inhibit the upwelling of poorly ventilated deep waters to the upper ocean (Gnanadesikan et al., 2007; Takano et al., 2018). This mechanism is mainly restricted to the equatorial and eastern boundary upwelling regions above the thermocline, but cannot explain the basin-wide ventilation improvement at low latitudes below the thermocline (Fig. 1b). Thus, alternative mechanisms are needed to account for the widespread enhancement of ventilation in the tropical subsurface under climate warming. In this study, we analyze 21st-century climate model simulations from the Coupled Model Intercomparison Project phase 6 (CMIP6; Eyring et al., 2016) to investigate the

projected changes in oxygen and ventilation. Our analyses reveal that the ventilation

enhancement in the tropical subsurface is related to a basin-wide deepening of the upper ocean isopycnals. To elucidate the underlying mechanisms, we conduct a suite of process-based ocean-only simulations and demonstrate that the basin-wide isopycnal deepening is driven by surface warming and freshening in the extratropics. These extratropical changes induce anomalous cross-hemispheric overturning responses, which push well-ventilated and oxygen-rich shallower waters to greater depths, resulting in improved oxygenation in the tropical subsurface. While similar processes also operate in the subtropics and high latitudes, their influences are largely offset by reduced subductions of mode and intermediate waters. Here, we highlight a hitherto under-explored mechanism that contributes to tropical subsurface oxygen increases, hinging on remote extratropical warming and freshening that enhances ventilation of the tropical subsurface ocean.

# Results

# Subsurface oxygen trends set by ventilation changes

We investigate the projected oxygen trends over the 21<sup>st</sup> century under the highemission scenario ("ssp5-8.5", O'Neill et al., 2016), as simulated by CMIP6 Earth system models (See "CMIP6 Models" in Methods). Our analysis focuses on waters at 100–500 m depths, where the most pronounced O<sub>2</sub> increases in tropical subsurface are projected (Supplementary Figs. S1 & S2d–f). While rising global ocean temperatures decrease the oxygen solubility in seawater (Supplementary Fig. S3b) and contribute to widespread deoxygenation across much of the global ocean (Fig. 1a), we observe an opposite trend at low latitudes: oxygen concentrations are increased in subsurface waters in the Atlantic and Indian Oceans and the eastern tropical North/South Pacific

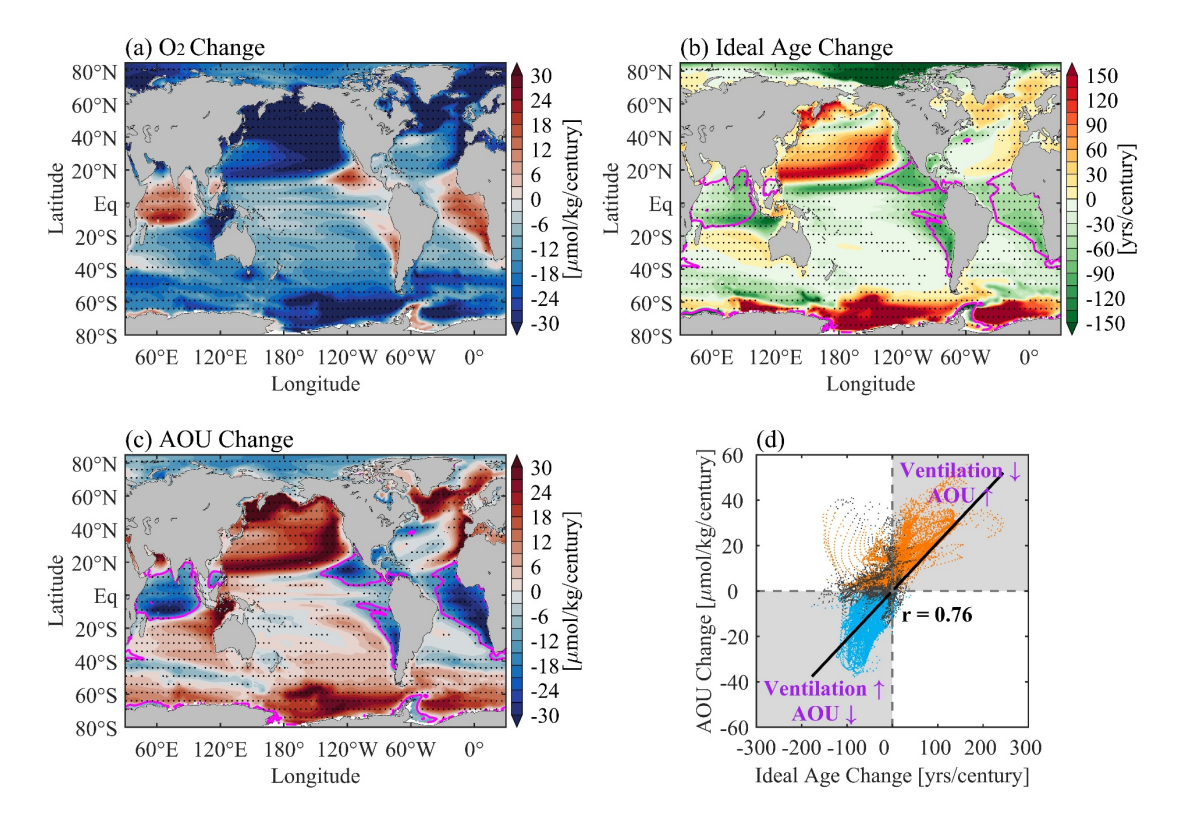


Figure 1. Oxygen and ventilation trends over the  $21^{st}$  century projected by CMIP6 models. Multimodel ensemble-mean trends in (a) oxygen concentration, (b) ideal age, and (c) AOU, averaged vertically between 100-500 m water depths. The ideal age represents the average time elapsed since the last contact with the atmosphere. The  $21^{st}$  century change is calculated as the linear trend over 2015-2100. Stippling in (a)–(c) indicate over three quarters of the examined models agree on the sign of changes. The magenta solid contours in (b) and (c) mark the regions with oxygen increases as shown in (a). (d) AOU changes vs. ideal age changes. The black line is a linear regression, with a correlation coefficient of r = 0.76. Each point represents a grid box of  $1^{\circ}\times1^{\circ}$  in (b) and (c). Dots in blue (AOU decrease) and orange (AOU increase) represent data with over 75% of the examined models agreeing on the sign of changes, while other data are shown by grey dots.

(Fig. 1a; Supplementary Fig. S2d-f). These low-latitude oxygen increases are caused by a reduced oxygen consumption, as indicated by the negative trends in apparent oxygen utilization (A0U) in these regions (Fig. 1c; see "Oxygen consumption and ventilation age" in Methods).

Both biological and physical processes contribute to the declining oxygen consumption in the tropical subsurface. The export of organic matter from the surface euphotic zone to the subsurface, represented by the downward flux of particulate organic carbon at 100 m water depth, declines in most regions during the 21<sup>st</sup> century (Supplementary Fig. S4a), consistent with published projections (Bopp et al., 2013;

Kwiatkowski et al., 2020; Ryan-Keogh et al., 2025). This decline in organic matter export would be accompanied with decreased remineralization and, consequently, a reduced oxygen consumption in the tropical subsurface. Concurrently, ventilation strengthens with an effect to enhance oxygenation in the tropical subsurface. We also note that ventilation substantially weakens and decreases subsurface oxygen levels in the Southern Ocean and the North Pacific subtropical regions (Fig. 1b). While biological changes lower *AOU* in the tropical subsurface, the spatial structure of *AOU* trends on global scales appear to be largely governed by changes in the ventilation state rather than by the biological consumption (Fig. 1d vs. Supplementary Fig. S4b).

# Enhanced tropical subsurface ventilation due to basin-wide isopycnal deepening

Enhanced ventilation in the tropical subsurface ocean is unexpected from a warming climate. Ventilations of the subsurface ocean, taking place primarily in high-and mid-latitude regions, occur through a few interconnected processes, including the formation of deep/bottom waters, subduction of mode/intermediate waters, and lateral transport by ocean circulations (Morrison et al., 2022). Climate warming increases upper-ocean stratification, reducing the formation of deep and bottom waters (Purkey and Johnson, 2013; Weijer et al., 2020; Li et al., 2023) and weakening mode and intermediate water subduction (Downes et al., 2009; Luo et al., 2009). Of relevant to this study, the ventilation will be suppressed in the ocean interior affected by mode/intermediate waters (Fig. 1b; Supplementary Fig. S2j–l). This is manifested by pronounced ventilation age increases in the subtropics and subpolar regions (Fig. 1b).

By contrast, ventilation changes in the tropical subsurface (100–500 m), where the thermocline's "shadow zones" are located (Luyten et al., 1983), are primarily controlled by an imbalance between vertical advection and diffusion (Gnanadesikan et al., 2007). Characterized by a shallow thermocline, the modern tropical subsurface is not directly affected by mode/intermediate water subduction, but instead occupied by waters older than subtropical subsurface waters (Supplementary Figs. S2g–1 & S5). Based on our decomposition of ventilation age and AOU changes (See "Decomposition of AOU and ideal age" in Methods), we show that ventilation age reductions and negative AOU

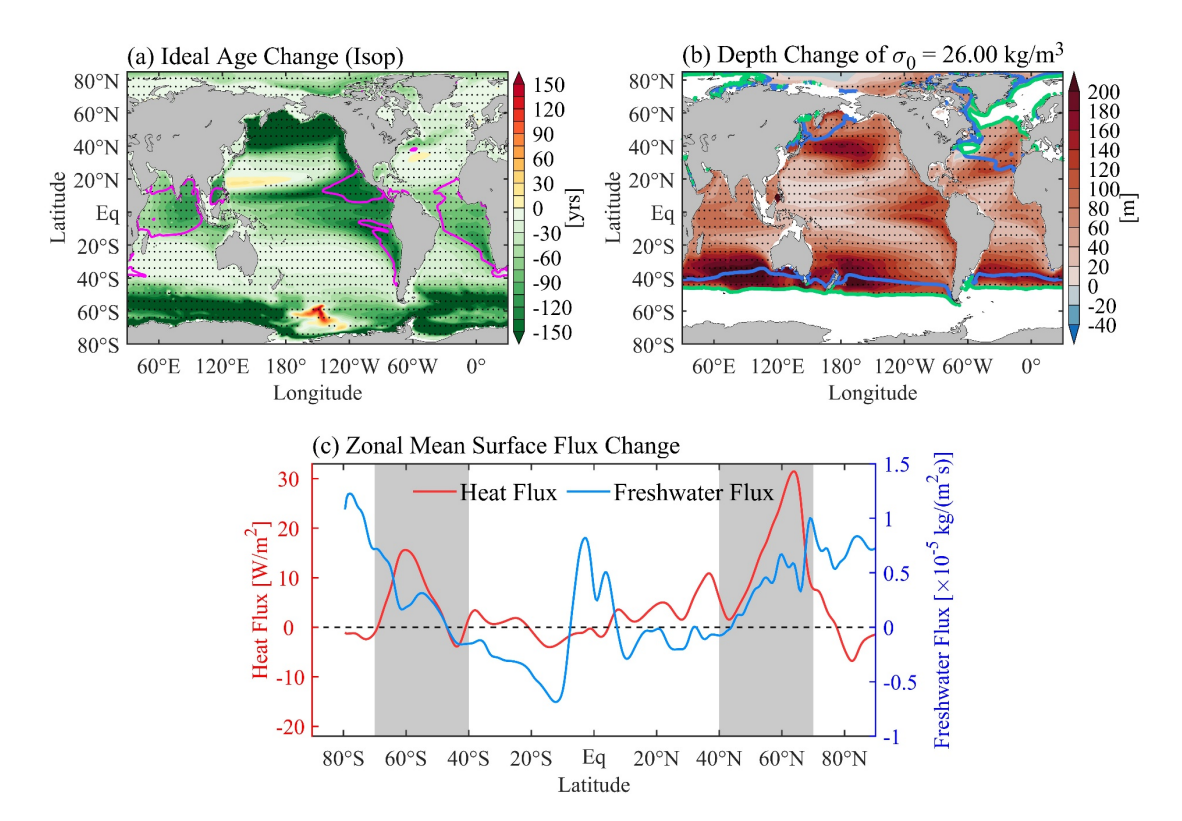


Figure 2. Ideal age changes due to isopycnal deepening. (a) Ideal age changes due to vertical movements of isopycnal surfaces, averaged vertically over 100-500 m water depths (See "Decomposition of AOU and ideal age" in Methods). Magenta contours mark the region where oxygen concentration increases as shown by multi-model mean (Fig. 1a). (b) Depth changes of the isopycnal,  $\sigma_0 = 26.00 \, kg/m^3$ , from years 2015-2019 to 2096-2100. The solid blue and green contours represent outcropping locations of the isopycnal,  $\sigma_0 = 26.00 \, kg/m^3$ , defined as the isopycnal reaching the bottom of surface mixed layer, during 2015-2019 and 2096-2100, respectively. Regions are stippled where over 75% of the models agree on the sign of changes. (c) Zonal-mean changes in multi-model mean surface net heat flux and surface net freshwater flux over the 21<sup>st</sup> century. Positive values represent fluxes into the ocean. The shading indicates extratropical regions with increased heat and freshwater fluxes under future warming.

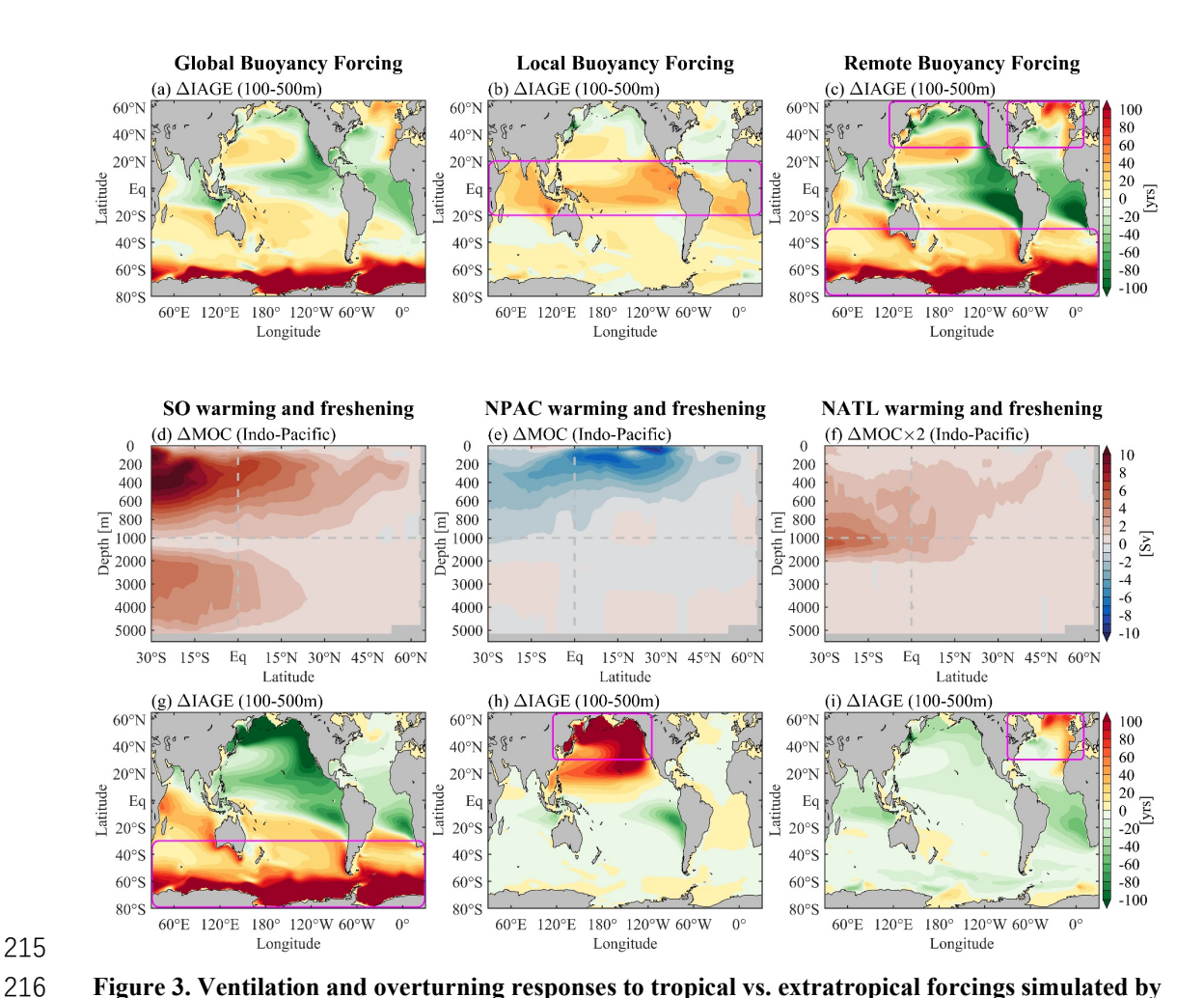
trends in the tropical subsurface are largely driven by deepening of isopycnal surfaces under climate warming over the 21<sup>st</sup> century (Figs. 1b & 2a; Supplementary Fig. S6), consistent with previously findings (Takano et al., 2018). As the climate warms, isopycnal surfaces move progressively to greater depths (Fig. 2b; Supplementary Fig. S7), and consequently the upper ocean is replaced with lighter and younger water masses (Fig. 2a; Supplementary Fig. S7). Critically, this deepening of isopycnal surfaces is not confined to the tropics, but a basin-scale feature that culminates at midlatitudes particularly in the Southern Ocean and North Pacific (Fig. 2b; Supplementary

Fig. S7). Nevertheless, subsurface waters in the subtropics are overall characterized by weakened ventilations, owing to suppressed production of mode/intermediate waters in mid-latitude and subpolar regions.

Regarding physical mechanisms, the basin-scale deepening of an isopycnal surface,  $\sigma$ , is unlikely driven by wind changes which only redistribute water volume within ocean basins (Huang, 2015). Instead, it is driven by an anomalous water mass transformation from subsurface to density classes lighter than  $\sigma$  (See "Isopycnal" deepening driven by water mass transformation" in Methods). This transformation likely occurs at the outcropping positions of the isopycnal surface (blue and green contours in Fig. 2b) in the Southern Ocean, North Pacific, and North Atlantic. Indeed, climate models project increased surface heat and freshwater fluxes into the ocean poleward of 40° latitude in both hemispheres as the climate warms (Liu et al., 2021; Fig. 2c; Supplementary Fig. S8). Surface warming and freshening (Supplementary Fig. S9) drive anomalous surface water mass transformation from dense to light waters, leading to volume convergence in the upper ocean. This anomaly may propagate equatorward and then into the other hemisphere along the boundaries and equator in the form of Kelvin waves, establishing cross-hemispheric overturning circulation responses (Sun et al., 2020; Luongo et al., 2025). These processes result in basin-scale deepening of isopycnal surfaces (Fig. 2b; Supplementary Fig. S7).

# Enhanced ventilation driven by extratropical buoyancy forcing

We use MITgcm to conduct a set of process-oriented numerical experiments to illustrate the role of extratropical forcing in tropical ventilation changes (see "MITgcm simulations" in Methods). Under global surface wind and buoyancy forcings (e.g., warming and freshening) derived from a coupled CESM2 experiment with increasing atmospheric CO<sub>2</sub>, our MITgcm run largely reproduces the structure of ventilation changes shown by CMIP6 and CESM2, with enhanced ventilation in the tropical subsurface and weakened ventilation in the subtropics and at high latitudes (Supplementary Fig. S10). By replacing surface wind or buoyancy forcing the preindustrial conditions, we show that the enhanced ventilation in the tropical



**Figure 3.** Ventilation and overturning responses to tropical vs. extratropical forcings simulated by MITgcm. (a)–(c) Ventilation changes driven by surface warming and freshening applied (a) globally, (b) in low latitudes, and (c) in the extratropics. (d–f) Indo-Pacific overturning circulation and (g–i) upper ocean (100–500 m) ventilation responses to surface warming and freshening applied to the (d, g) Southern Ocean, (e, h) North Pacific, and (f, i) North Atlantic. Magenta boxes denote the regions where surface buoyancy forcing perturbations are applied. Ideal ages represent averages over 100–500 m depths at 100 years after perturbations. Ventilation changes under extratropical buoyancy forcings (c) are the sum of ventilation changes shown in (g–i). Positive streamfunction indicates clockwise overturning circulation anomaly. The overturning response in (f) is multiplied by 2 for better presentation. For details, see "MITgcm simulations" in Method.

subsurface can be attributed to changes in surface buoyancy forcing (Fig. 3a; Supplementary Fig. S11a-c). This contrasts with historical oxygen changes in the tropical subsurface on decadal and multi-decadal timescales, which are primarily driven by local wind changes associated with climate mode variability (Deutsch et al., 2011; Duprey et al., 2024; Pichevin et al., 2024).

When surface warming and freshening are applied exclusively to low latitudes

(20°S–20°N), our simulations show increased ventilation age in the tropical subsurface (Fig. 3b) despite a slight deepening of isopycnal surfaces (Supplementary Fig. S12e), contrary to previous expectations (Gnanadesikan et al., 2007; Takano et al., 2018). Our simulated subsurface aging occurs because enhanced surface stratification weakens the shallow overturning circulation at low latitudes (Supplementary Fig. S13d), the primary means to ventilate the tropical subsurface (McCreary and Lu, 1994; Liu, 1994). Additionally, stronger surface stratification may cause thermocline shoaling in tropical regions, expanding the poorly ventilated shadow zone (Luyten et al., 1983).

When applying surface warming and freshening to extratropical regions (30° latitude poleward), the ventilation age substantially decreases in the tropical subsurface (Fig. 3c). This occurs as the extratropical warming and freshening drive crosshemispheric overturning responses (Fig. 3d-f; Supplementary Fig. S14) associated with basin-wide deepening of isopycnal surfaces (Supplementary Fig. S12g-i). To illustrate this mechanism, we have applied surface warming and freshening to the Southern Ocean, North Pacific, and North Atlantic, separately. We find that surface warming and freshening in the Southern Ocean induces a clockwise, cross-hemispheric overturning circulation response in the upper 1 km of the Indo-Pacific and Atlantic oceans (Fig. 3d; Supplementary Fig. S14a). The overturning response is characterized by anomalous northward volume transport in the upper 300 m, coupled with a deepening of isopycnal surfaces (Supplementary Fig. S12g). The resulting downward transport of wellventilated waters substantially decreases ventilation age in the north and tropical Pacific, North Indian and Atlantic (Fig. 3g). Concurrently, the subsurface ventilation age increases in the Southern Hemisphere subtropical gyres due to reduced subduction of mode/intermediate waters in the Southern Ocean (Fig. 3g).

Similarly, applying surface warming and freshening in the North Pacific causes an anticlockwise overturning response (Fig. 3e), which is also accompanied with basin-wide deepening of isopycnals (Supplementary Fig. S12h). This isopycnal deepening decreases subsurface ventilation age in the southern Indo-Pacific (Fig. 3h), although by a small magnitude due to relatively weak vertical ideal age gradients in the Southern Hemisphere (Supplementary Fig. S2g). The reduced subduction of mode and

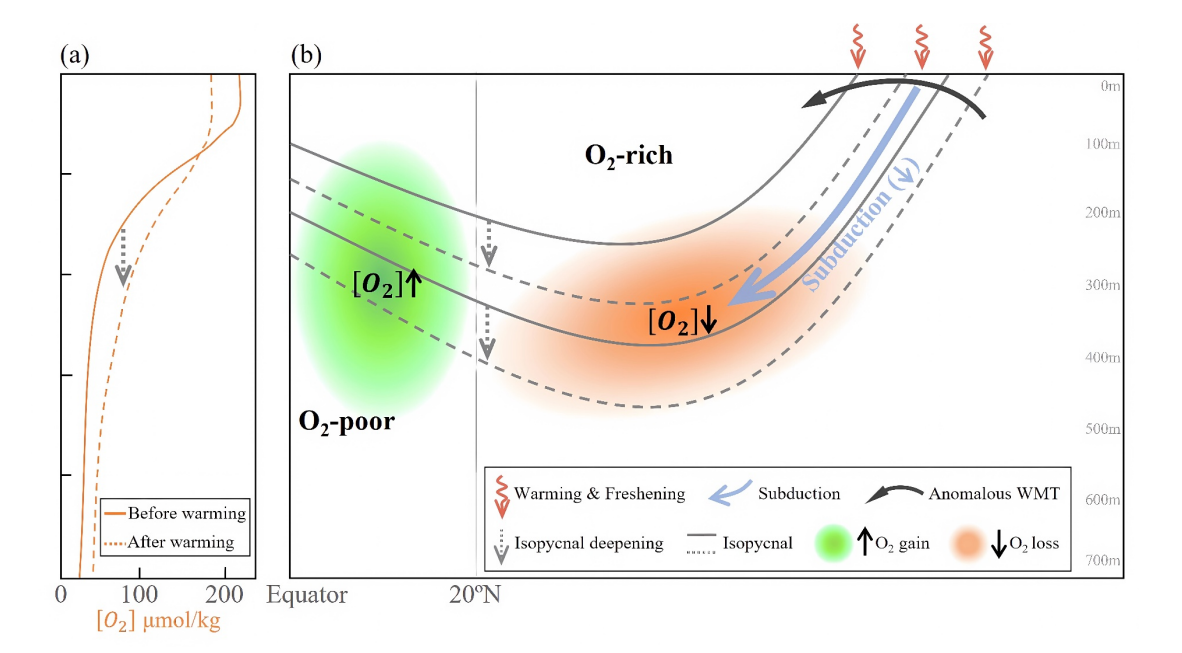


Figure 4. Schematic showing subsurface ventilation and oxygenation responses to extratropical warming and freshening. (a) Typical vertical oxygen profiles before (solid line) and after (dashed line) warming in the tropics, due to isopycnal deepening (vertical dashed arrow). (b) Subsurface oxygen changes forced by extratropical warming and freshening (red wavy arrows), which drives anomalous water mass transformation (WMT; long black arrow) from dense to light waters and results in basin-scale deepening (vertical dashed arrow) of isopycnals. Solid and dashed contours represent isopycnal surfaces before and after warming, respectively. The basin-scale isopycnal deepening brings well-ventilated, oxygen-rich shallower waters to greater depths, improving ventilation and increasing oxygen (green shading) in the tropical subsurface. By contrast, the subtropical subsurface, which is ventilated by subduction of mode and intermediate waters (long blue arrow), is expected to lose oxygen (orange shading) because the reduced subduction (blue downward arrow) and associated ventilation weakening overwhelms the impacts of isopycnal deepening under climate warming. The schematic shows the Northern Hemisphere, but similar mechanisms also apply to the Southern Hemisphere. The pattern of oxygen and ventilation changes depicted here are consistent with and supported by analyses of CMIP model outputs (Supplementary Fig. S15).

intermediate waters in the North Pacific increases ventilation age in the North Pacific (Fig. 3h).

Extratropical heat/freshwater forcing in the North Atlantic also leads to ventilation changes in tropical subsurface waters via weakening of the Atlantic meridional overturning circulation (AMOC) and associated overturning responses across ocean basins (Fig. 3f; Supplementary Fig. S14c). As the AMOC weakens, a clockwise overturning anomaly develops in the Indo-Pacific (Fig. 3f), associated with deepening

of isopycanl surfaces (Supplementary Fig. S12i; Sun et al., 2020; Sun and Thompson, 2020). This cross-basin response, more pronounced at greater depths (200-2000 m; Fig. 3f), decreases subsurface ventilation age across much of the global ocean (Fig. 3i).

With combined extratropical warming and freshening forcings in both hemispheres, the upper ocean develops anomalous overturning circulation that is associated with basin-wide deepening isopycnal surfaces (Supplementary Fig. S13c, e), which effectively pushes down well-ventilated shallow waters and thereby decreases subsurface ventilation age in the tropics. These processes primarily modulate ventilation and oxygenation changes in the tropical subsurface which is not directly affected by subduction of mode/intermediate waters formed at higher latitudes. By contrast, subsurface waters in subtropical regions are tightly affected by thermocline circulation and their ventilation ages are projected to increase due to reduced subduction of mode and intermediate waters in response to future warming.

# **Discussion**

Our study reveals that the enhanced ventilation and oxygenation in the tropical subsurface under anthropogenic warming, as projected by most climate models, is largely forced by extratropical warming and freshening. These extratropical changes drive cross-hemispheric overturning adjustments that enhance tropical subsurface ventilation primarily at 100–500 m water depths (Fig. 4), although mode and intermediate water subduction is reduced due to intensified surface stratification at midlatitudes.

Extratropical warming and freshening suppress surface water mass transformation into mode and intermediate waters, inducing upper-ocean volume convergence. The convergence propagates equatorward and across hemispheres via wave processes, establishing cross-hemispheric overturning responses which deepen isopycnal surfaces basin-wide and bring younger, oxygen-rich shallow waters to greater depths. This process enhances subsurface ventilation, particularly at low latitudes (Fig. 4, green; Supplementary Fig. S15). Alongside reduced biological oxygen consumption (although currently difficult to quantify with confidence), the enhanced ventilation contributes

substantially to the projected subsurface oxygenation in the tropics. In comparison, the impacts of ispycnal deepening on subtropical subsurface O<sub>2</sub> levels are overwhelmed by reduced subduction of mode/intermediate waters (Fig. 4, orange; Supplementary Fig. S15). Thus, subtropical subsurface waters deoxygenate more rapidly than their tropical counterparts under future warming (Bopp et al., 2013; Kwiatkowski et al., 2020; Busecke et al., 2022; Ditkovsky and Resplandy, 2025).

Our proposed mechanisms provide a new perspective for past and future oxygen dynamics. Paleoclimate records document millennial-scale fluctuations of subsurface oxygen levels in the low-latitude Indo-Pacific which are coherent with North Atlantic temperature oscillations during the last glacial period (Schmittner et al., 2007, 2008). The AMOC weakening and concurrent Southern Hemisphere warming during stadials (cold time periods) (Stocker and Johnsen, 2003) possibly triggered cross-hemispheric overturning responses and isopycnal deepening, contributing to the reconstructed coupling between AMOC and the Indo-Pacific tropical subsurface oxygenation on millennial scales (Schmittner et al., 2008). Under anthropogenic forcing, tropical subsurface oxygenation may contract oxygen minimum zones (Busecke et al., 2022). Nevertheless, it is important to note that tropical subsurface responses occur on centennial-scales, because ocean interior diapycnal mixing ultimately counterbalances the anomalous water mass transformation in the extratropics and halts the basin-wide isopycnal deepening (Sun et al., 2020). Our MITgcm simulations show that the enhanced ventilation in the tropical subsurface diminishes over centuries (Supplementary Fig. S16), foreshadowing marine ecosystem's long-term vulnerability to deoxygenation.

In addition to anthropogenic forcing, subsurface O<sub>2</sub> levels are also modulated by natural climate variability, which may obscure the emergence of tropical subsurface oxygenation signals under future warming. For example, wind shifts may drive decadal tropical subsurface O<sub>2</sub> level fluctuations (Deutsch et al., 2011; Duprey et al., 2024; Pichevin et al., 2024) until their effects are exceeded by anthropogenic forcings. To better project transient responses of tropical subsurface oxygenation, it is valuable to improve model fidelity in extratropical processes, because simulation biases in mid-

latitude air-sea fluxes and eddy-mediated water mass transformations propagate directly into uncertainties in cross-hemispheric adjustments (Ma et al., 2016). Optimizing relevant physical processes in models is essential for reliable predictions of subsurface oxygen levels, with critical implications for future marine ecosystems.

349

350

351

352

353

354

355

356

357

358

359

360

361

348

345

346

347

#### Methods

# CMIP6 models used in this study

We use outputs from 19 climate models, participating the Coupled Model Intercomparison Project, Phase 6 (CMIP6; Eyring et al., 2016), to investigate the projected oxygen changes over the 21st century. For each model with multiple ensemble members, we choose only one member in our analyses (Supplementary Tab. S1). We approximate ventilation age with ideal age, which represents the average time elapsed since the water mass was last in contact with the atmosphere. Note that we only used 9 models for ventilation age analysis -- ideal age shows substantial biases in 5 models, including ACCESS-ESM1-5, IPSL-CM6A-LR, MPI-ESM1-2-HR, MRI-ESM2-0, and UKESM1-0-LL. We focus on the experiments under high-emission scenario (ssp5-8.5; O'Neill et al., 2016), during 2015–2100.

362

363

364

365

366

367

368

371

372

373

# Oxygen consumption and ventilation age

Dissolved oxygen is progressively depleted by respiration after water masses leave the ocean surface. We use Apparent Oxygen Utilization (AOU) to approximate the cumulative oxygen consumption due to biological processes (Ito et al., 2004). In practice, AOU is defined as the difference between the saturated oxygen concentration,  $[O_2^{sat}]$ , and the local oxygen concentration,  $[O_2]$ , i.e.,

$$AOU = [O_2^{sat}] - [O_2], (1)$$

where  $[O_2^{sat}]$  is calculated from local temperature and salinity.

If we neglect the air-sea disequilibrium effect, AOU can be considered as the integration of oxygen consumption rate  $(S_{OUR})$  by biological respiration along the ventilation pathway connecting the subduction site to the ocean interior, i.e.,

$$AOU = \int_C S_{OUR} dt = \bar{S}_{OUR} I, \qquad (2)$$

where  $\bar{S}_{OUR}$  denotes the mean oxygen consumptions along the ventilation pathway and I represents ventilation age. This equation allows us to link changes in AOU to variations in either biological respiration rate or ventilation age, providing insights into the drivers of oxygen changes. In climate projections for the  $21^{\text{st}}$ -century, a decline in organic matter export (Supplementary Fig. S4a) suggests a smaller oxygen consumption rate in a warming climate, i.e.,  $\Delta S_{OUR} < 0$ . The decreasing ventilation age in the tropical subsurface,  $\Delta I < 0$ , also contributes to the negative AOU trends (Fig. 1b, c).

# Decomposition of AOU and ideal age

Ventilation and oxygen changes in the tropical subsurface under climate warming are primarily controlled by an imbalance between vertical advection and diffusion (Gnanadesikan et al., 2007). Changes in vertical advection can be driven by both adiabatic processes and diabatic mixing. However, on decadal to centennial timescales, vertical movements below the thermocline, i.e., vertical advection, are predominantly adiabatic, associated with vertical movements of isopycnal surfaces (Sun et al., 2022). Here we decompose the 21<sup>st</sup>-century changes in *AOU* and ideal age into contributions due to vertical movements of isopycnal surfaces vs. other processes, such as horizontal advection and mixing along/across isopycnals.

Changes in a passive tracer, c, which can be either AOU or ideal age, can be written as follows,

$$\Delta c_{Total} = \Delta c_{isop} + \Delta c_{res}, \tag{3}$$

where  $\Delta c_{isop}$  is the tracer change due to vertical isopycnal movements and  $\Delta c_{res}$  represents the remaining change due to other processes. We quantify the change due to vertical isopycnal movements at depth, z, as

400 
$$\Delta c_{isop}(z) = c_0(\zeta) - c_0(z), \tag{4}$$

Here  $c_0$  represents the tracer distribution averaged over 2015–2019 and  $\zeta$  is the depth of isopycnal,  $\sigma$ , at the same period that satisfies

Where  $\rho_0$  and  $\rho_1$  represent density profiles averaged over 2015–2019 and 2096–405 2100, respectively.

The decomposition reveals that the enhanced ventilation and negative AOU trend in the tropical subsurface can be largely attributed to the vertical deepening of isopycnal surfaces (Supplementary Fig. S6). Conversely, in the subtropics, the weakened ventilation and positive AOU trends are primarily driven by other processes that outweigh the effects of isopycnal deepening (Supplementary Fig. S6).

# Isopycnal deepening driven by water mass transformation

To identify the processes that drive the basin-wide deepening of isopycnals, we examine the volume budget in isopycnal coordinates (Fig. 4). The volume V above an isopycnal surface,  $\sigma$ , is governed by a balance between interior diapycnal transport,  $G_{diap}$ , and surface water mass transformation at the outcropping locations,  $G_{sfc}$ :

$$\frac{dV}{dt} = G_{diap} + G_{sfc},\tag{6}$$

Under climate warming, the isopycnal surfaces deepen across ocean basins (Fig. 2b), i.e., dV/dt > 0. This indicates an enhanced transformation of water from below the isopycnal into the upper ocean, which can occur either in the interior or at the surface outcropping regions. However, diapycnal mixing is weak below the surface mixed layer (Polzin et al., 1997). Thus, substantial changes in  $G_{diap}$  would require large modifications to the density structure (Munk, 1966) and are therefore unlikely to dominate the volume increases (Sun et al., 2020). In contrast, the basin-scale deepening of isopycnals is more plausibly driven by changes in surface water mass transformation at the outcropping latitudes, as shown by the MITgcm simulations.

# **MITgcm simulations**

We carry out a suite of idealized ocean-only experiments to investigate the role of different surface forcing configurations in driving oxygen changes under climate warming. The model, Massachusetts Institute of Technology General Circulation Model (MITgcm), uses a nonlinear equation of state (Jackett and Mcdougall, 1995). The model resolution is 1° in longitude and 0.5° in latitude. The model domain excludes the Arctic to avoid the singularity problem in the polar region. In the vertical, there are 30 layers ranging from 10 m at the top to 369 m at the bottom. Vertical mixing is handled by the K-Profile parameterization (Large et al., 1994). Unresolved eddies are represented using the skew-flux of the Gent-McWilliams parameterization with a background diffusivity of 1000 m²/s (Griffies, 1998). Isopycnal diffusion due to eddies is parameterized using the Redi scheme with a diffusivity of 1,000 m²/s (Redi, 1982).

In our MITgcm simulations, surface forcing for temperature includes a relaxation to a prescribed monthly sea surface temperature field, with a relaxation timescale of 14 days (Haney, 1971), and a net surface heat flux. Surface salinity is forced by monthly surface freshwater flux, which includes contributions due to precipitation, evaporation, sea ice melting/formation, and river runoff. A weak relaxation of the surface salinity to a prescribed climatology is also included to avoid possible bi-stability of the overturning circulation due to the mixed boundary conditions (Stommel, 1961). Ideal age is included in the model as a passive tracer that is restored to zero at the sea surface. Surface forcing fields for our MITgcm simulations are derived from two fully coupled simulations by the NCAR CESM2 model (Danabasoglu et al., 2020): piControl and 4×CO<sub>2</sub> (Supplementary Fig. S17a–h). In CESM2 piControl, the atmospheric CO<sub>2</sub> is kept at the pre-industrial level. The CESM2 4×CO<sub>2</sub> experiment is initialized from piControl and continued for 1000 years, but with the atmospheric CO<sub>2</sub> instantaneously quadruped at the beginning of simulation. Ventilation changes in 4×CO<sub>2</sub> resemble the 21<sup>st</sup>-century changes in CMIP6 (Supplementary Fig. S10; years 190–200).

A total of eight experiments were carried out using the MITgcm ocean model: "Control", "4×CO<sub>2</sub>", "Wind", "Buoyancy", "LowLat", "SO", "NATL", and "NPAC". In "Control" run, both surface wind and buoyancy forcing (surface heat flux, surface temperature, surface freshwater flux, and surface salinity) are taken from CESM2 piControl (Supplementary Fig. S17a–d). "Control" is run for over 3,000 years to achieve an approximately steady state. The other seven experiments are initialized from

the end of "Control" and continued for over 500 years. In "4×CO<sub>2</sub>", both surface wind and buoyancy forcing are taken from CESM2 4×CO<sub>2</sub> (monthly climatology over years 150–200). In "Wind", surface wind is taken from CESM2 4×CO<sub>2</sub> but surface buoyancy forcing is kept the same as in "Control". In "Buoyancy", surface wind is kept the same as in "Control" but surface buoyancy forcing is taken from CESM2 4×CO2 (Supplementary Fig. S17e-h). Thus, the difference between "Buoyancy" and "Control" represents the oceanic responses to global surface warming and freshening perturbations. In the other four experiments, surface forcing configurations are like "Buoyancy" but the surface buoyancy forcing perturbations (warming and freshening; Supplementary Fig. S17i-l) are applied only in specific regions rather than globally. In "LowLat", surface warming and freshening are applied only within 20°S-20°N. Outside of this region, surface buoyancy forcing are kept the same as in "Control". The transition in surface buoyancy forcing from 4×CO<sub>2</sub> to piControl takes place gradually over 10° latitudes at around the boundary (20°S and 20°N) to avoid spurious jump in surface forcing. Similar approach applies when we apply surface warming and freshening only in the Southern Ocean (south of 30°S, "SO"), North Pacific (north of 30°N, "NPAC"), and North Atlantic (north of 30°N, "NATL"). Our MITgcm simulations under global surface warming and freshening ("4×CO2" - "Control") largely reproduces the structure of overturning and ventilation changes in CESM2 and CMIP6 multi-model mean (Supplementary Fig. S10; Fig. S13). The ocean develops a shallow cross-hemispheric overturning circulation response when extratropical warming and freshening are applied in one hemisphere (Fig. 3; Supplementary Fig. S14). These overturning responses effectively push well-ventilated water to greater depths and decrease ventilation age, primarily in the tropical subsurface ocean. When combined together, the remote extratropical warming and freshening drive shallow overturning circulation responses that are roughly antisymmetric about the equator (Supplementary Fig. S13c, e) and causes ventilation changes that approximately reproduces the spatial structure in CMIP6 and CESM2 (Supplementary Fig. S10).

462

463

464

465

466

467

468

469

470

471

472

473

474

475

476

477

478

479

480

481

482

483

484

485

486

487

488

489

492	Data availability			
493	The CMIP6 model output was downloaded from the Earth System Grid Federation			
494	node ( <a href="https://esgf-node.llnl.gov/projects/esgf-llnl/">https://esgf-node.llnl.gov/projects/esgf-llnl/</a> ). Model outputs from the MITgcm			
495	experiments will be made publicly available from the online open access repository,			
496	Figshare. Source data are provided in this paper.			
497				
498	Code availability			
499	The code for reproducing the ocean ventilation responses (MITgcm experiments)			
500	in this study is made publicly available from the online open-access repository, Figshare			
501	with <a href="https://doi.org/10.6084/m9.figshare.26129629">https://doi.org/10.6084/m9.figshare.26129629</a> .			
502				
503	Acknowledgements			
504	Without implying their endorsement, we are grateful for helpful discussions with			
505	Lynne Talley, Benjamin Taylor, and Yan Du. S.S. and J.Y. acknowledge support from			
506	NSF China (42330403) and Laoshan Laboratory (LSKJ202400203).			
507				
508	Author contributions			
509	S. S. conceived this study and carried out the MITgcm simulations. Z.G. led the			
510	analysis. Z.G. and S.S. drafted the manuscript. D.S., J.Y., and L.W. contributed to			
511	discussions and improving the manuscript.			
512				
513	Competing interests			
514	The authors declare no competing interests.			
515				
516	Reference			
517 518 519	Babbin, A. R., Bianchi, D., Jayakumar, A., and Ward, B. B. (2015). Rapid nitrous oxide cycling in the suboxic ocean. <i>Science</i> , 348(6239), 1127–1129. <a href="https://doi.org/10.1126/science.aaa8380">https://doi.org/10.1126/science.aaa8380</a>			
520 521 522	Bakker, P., Schmittner, A., Lenaerts, J. T. M., Abe-Ouchi, A., Bi, D., van den Broeke, M. R., Chan, WL., Hu, A., Beadling, R. L., Marsland, S. J., Mernild, S. H., Saenko, O. A., Swingedouw, D., Sullivan, A., and Yin, J. (2016). Fate of the			

- 523 Atlantic Meridional Overturning Circulation: Strong decline under continued
- warming and Greenland melting. Geophysical Research Letters, 43(23), 12252–
- 525 12260. https://doi.org/10.1002/2016GL070457
- Bopp, L., Quéré, C. L., Heimann, M., Manning, A. C., and Monfray, P. (2002). Climate-
- 527 induced oceanic oxygen fluxes: Implications for the contemporary carbon budget.
- 528 Global Biogeochemical Cycles, 16(2), 6–1–6–
- 529 13. https://doi.org/10.1029/2001gb001445
- Bopp, L., Resplandy, L., Orr, J. C., Doney, S. C., Dunne, J. P., Gehlen, M., Halloran, P.,
- Heinze, C., Ilyina, T., Séférian, R., Tjiputra, J. and Vichi, M. (2013). Multiple
- stressors of ocean ecosystems in the 21st century: projections with CMIP5 models.
- 533 *Biogeosciences*, 10, 6225–6245. <a href="https://doi.org/10.5194/bg-10-6225-2013">https://doi.org/10.5194/bg-10-6225-2013</a>
- Bopp, L., Resplandy, L., Untersee, A., Le Mezo, P., and Kageyama, M. (2017). Ocean
- (de)oxygenation from the Last Glacial Maximum to the twenty-first century:
- insights from Earth System models. Philosophical Transactions of the Royal
- 537 Society A: Mathematical, Physical and Engineering Sciences, 375, 20160323.
- 538 http://dx.doi.org/10.1098/rsta.2016.0323
- Busecke, J. J. M., Resplandy, L., Ditkovsky, S. J., and John, J. G. (2022). Diverging
- fates of the Pacific Ocean oxygen minimum zone and its core in a warming world.
- 541 *AGU Advances*, 3(6), e2021AV000470. https://doi.org/10.1029/2021AV000470
- Capotondi, A., Alexander, M. A., Bond, N. A., Curchitser, E. N., and Scott, J. D. (2012).
- Enhanced upper ocean stratification with climate change in the CMIP3 models.
- Journal of Geophysical Research: Oceans, 117(C4), C04031.
- 545 <u>https://doi.org/10.1029/2011JC007409</u>
- Danabasoglu, G., Lamarque, J.-F., Bacmeister, J., Bailey, D. A., DuVivier, A. K.,
- Edwards, J., Emmons, L. K., Fasullo, J., Garcia, R., Gettelman, A., Hannay, C.,
- Holland, M. M., Large, W. G., Lauritzen, P. H., Lawrence, D. M., Lenaerts, J. T.
- M., Lindsay, K., Lipscomb, W. H., Mills, M. J., Neale, R., Oleson, K. W., Otto-
- Bliesner, B., Phillips, A. S., Sacks, W., Tilmes, S., van Kampenhout, L.,
- Vertenstein, M., Bertini, A., Dennis, J., Deser, C., Fischer, C., Fox-Kemper, B.,
- Kay, J. E., Kinnison, D., Kushner, P. J., Larson, V. E., Long, M. C., Mickelson, S.,
- Moore, J. K., Nienhouse, E., Polvani, L., Rasch, P. J., and Strand, W. G. (2020).
- The Community Earth System Model Version 2 (CESM2). *Journal of Advances in*
- 555 *Modeling Earth Systems*, 12(2), e2019MS001916.
- 556 https://doi.org/10.1029/2019MS001916
- Deutsch, C., Brix, H., Ito, T., Frenzel, H., and Thompson, L. (2011). Climate-forced
- variability of ocean hypoxia. Science, 333(6040), 336–339.
- 559 https://doi.org/10.1126/science.1202422
- 560 Ditkovsky, S., and Resplandy, L. (2025). Unifying future ocean oxygen projections
- using an oxygen water mass framework. Journal of Geophysical Research:
- 562 *Oceans*, 130, e2025JC022333. https://doi.org/10.1029/2025JC022333

- Downes, S. M., Bindoff, N. L., and Rintoul, S. R. (2009). Impacts of climate change on
- the subduction of Mode and Intermediate Water Masses in the Southern Ocean.
- Journal of Climate, 22(12), 3289–3302. <a href="https://doi.org/10.1175/2008JCLI2653.1">https://doi.org/10.1175/2008JCLI2653.1</a>
- 566 Duprey, N. N., Foreman, A. D., Carriquiry, J. D., Charles, C. D., Sanchez, S. C., Vonhof,
- H., Rubach, F., Rabenstein, R., Rohr, M., Reyes-Bonilla, H., Marconi, D., Sigman,
- D. M., Haug, G. H., and Martínez-García, A. (2024). Decadal oscillations in the
- ocean's largest oxygen-deficient zone. Science, 386(6725), 1019–1024.
- 570 https://doi.org/10.1126/science.adk4965
- 571 Eyring, V., Bony, S., Meehl, G. A., Senior, C. A., Stevens, B., Stouffer, R. J., and Taylor,
- K. E. (2016). Overview of the Coupled Model Intercomparison Project Phase 6
- (CMIP6) experimental design and organization. Geoscientific Model Development,
- 574 9(5), 1937–1958. https://doi.org/10.5194/gmd-9-1937-2016
- 575 Gnanadesikan, A., Dunne, J. P., and John, J. (2012). Understanding why the volume of
- suboxic waters does not increase over centuries of global warming in an Earth
- system model. *Biogeosciences*, 9(3), 1159–1172. <a href="https://doi.org/10.5194/bg-9-">https://doi.org/10.5194/bg-9-</a>
- 578 1159-2012
- 579 Gnanadesikan, A., Russell, J. L., and Fanrong, Z. (2007). How does ocean ventilation
- change under global warming? Ocean Science, 3(1), 43–53.
- 581 <u>https://doi.org/10.5194/os-3-43-2007</u>
- 582 Griffies, S. M. (1998). The Gent-McWilliams skew flux. Journal of Physical
- 583 *Oceanography*, 28(5), 831–841. https://doi.org/10.1175/1520-
- 584 <u>0485(1998)028<0831:TGMSF>2.0.CO;2</u>
- Haney, R. L. (1971). Surface thermal boundary condition for ocean circulation models.
- Journal of Physical Oceanography, 1(4), 241–248. https://doi.org/10.1175/1520-
- 587 0485(1971)001<0241:stbcfo>2.0.co;2
- Helm, K. P., Bindoff, N. L., and Church, J. A. (2011). Observed decreases in oxygen
- content of the global ocean. Global Biogeochemical Cycles, 38(23), 110–124.
- 590 https://doi.org/10.1029/2011GL049513
- Huang, R. X. (2015). Heaving modes in the world oceans. Climate Dynamics, 45,
- 592 3563–3591. https://doi.org/10.1007/s00382-015-2557-6
- 593 Ito, T., Follows, M. J., and Boyle, E. A. (2004). Is AOU a good measure of respiration
- in the oceans? Geophysical Research Letters, 31(17), L17305.
- 595 https://doi.org/10.1029/2004GL020900
- Ito, T., Minobe, S., Long, M. C., and Deutsch, C. (2017). Upper ocean O<sub>2</sub> trends: 1958–
- 597 2015. *Geophysical Research Letters*, 44(9), 4214–4223.
- 598 https://doi.org/10.1002/2017g1073613
- Jackett, D. R., and Mcdougall, T. J. (1995). Minimal adjustment of hydrographic
- profiles to achieve static stability. Journal of Atmospheric and Oceanic
- 601 Technology, 12(2), 381–389. <a href="https://doi.org/10.1175/1520-">https://doi.org/10.1175/1520-</a>

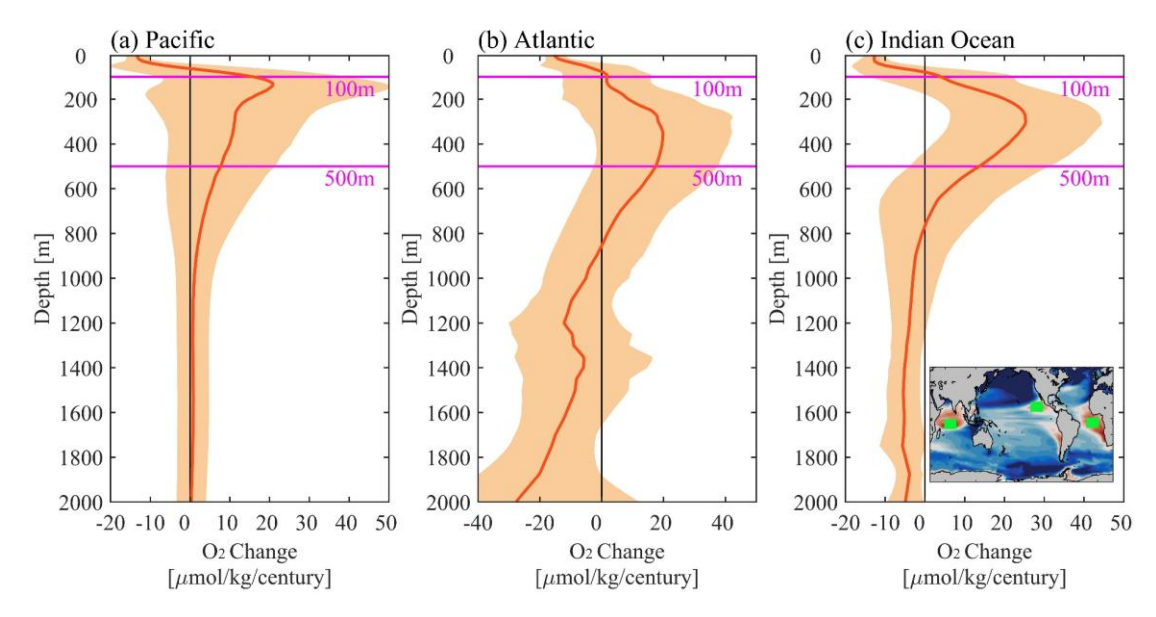
- Keeling, R. F., and Garcia, H. E. (2002). The change in oceanic O<sub>2</sub> inventory associated with recent global warming. *Proceedings of the National Academy of Sciences*, 99(12), 7848–7853. <a href="https://doi.org/10.1073/pnas.122154899">https://doi.org/10.1073/pnas.122154899</a>
- Keeling, R. F., Körtzinger, A., and Gruber, N. (2010). Ocean deoxygenation in a warming world. *Annual Review of Marine Science*, 2(1), 199–229. <a href="https://doi.org/10.1146/annurev.marine.010908.163855">https://doi.org/10.1146/annurev.marine.010908.163855</a>
- Kwiatkowski, L., Torres, O., Bopp, L., Aumont, O., Chamberlain, M., Christian, J. R., 609 Dunne, J. P., Gehlen., M., Ilyina, T., John, J. G., Lenton, A., Li, H., Lovenduski, 610 N. S., Orr, J. C., Palmieri, J., Santana-Falcón, Y., Schwinger, J., Séférian, R., Stock, 611 C. A., Tagliabue, A., Takano, Y., Tjiputra, J., Toyama, K., Tsujino, H., Watanabe, 612 M., Yamamoto, A., Yool, A., and Ziehn, T. (2020). Twenty-first century ocean 613 warming, acidification, deoxygenation, and upper-ocean nutrient and primary 614 production decline from CMIP6 model projections. Biogeosciences, 17, 3439-615 3470. https://doi.org/10.5194/bg-17-3439-2020 616
- Large, W. G., McWilliams, J. C. and Doney, S. C. (1994). Oceanic vertical mixing: a review and a model with a nonlocal boundary layer parameterization. *Reviews of Geophysics*, 32(4), 363–403. <a href="https://doi.org/10.1029/94RG01872">https://doi.org/10.1029/94RG01872</a>
- Li, G., Cheng, L., Zhu, J., Trenberth, K. E., Mann, M. E., and Abraham, J. P. (2020).
   Increasing ocean stratification over the past half-century. *Nature Climate Change*,
   10, 1116–1123. <a href="https://doi.org/10.1038/s41558-020-00918-2">https://doi.org/10.1038/s41558-020-00918-2</a>
- Li, Q., England, M. H., Hogg, A. M., Rintoul, S. R., and Morrison, A. K. (2023).
   Abyssal ocean overturning slowdown and warming driven by Antarctic meltwater.
   Nature, 615, 841–847. <a href="https://doi.org/10.1038/s41586-023-05762-w">https://doi.org/10.1038/s41586-023-05762-w</a>
- Liu, M., Vecchi, G., Soden, B., Yang, W., and Zhang, B. (2021). Enhanced hydrological
   cycle increases ocean heat uptake and moderates transient climate change. *Nature Climate Change*, 11, 848–853. <a href="https://doi.org/10.1038/s41558-021-01152-0">https://doi.org/10.1038/s41558-021-01152-0</a>
- Liu, Z. (1994). A simple model of the mass exchange between the subtropical and tropical ocean. *Journal of Physical Oceanography*, 24(6), 1153–1165. https://doi.org/10.1175/1520-0485(1994)024<1153:ASMOTM>2.0.CO;2
- Luo, Y., Liu, Q., and Rothstein, L. M. (2009). Simulated response of North Pacific Mode Waters to global warming. *Geophysical Research Letters*, 36(23), L23609, <a href="https://doi.org/10.1029/2009GL040906">https://doi.org/10.1029/2009GL040906</a>
- 635 Luongo, M. T., Xie, S., Eisenman, I., Sun, S., and Peng, Q. (2025). How the subsurface 636 tropical Pacific responds to subtropical surface cooling: Implications for cross-637 equatorial transport. *Journal of Climate*, 38(14), 3313–3331. 638 https://doi.org/10.1175/JCLI-D-24-0440.1
- 639 Luyten, J. R., Pedlosky, J., and Stommel, H. (1983). The ventilated thermocline.
  640 *Journal of Physical Oceanography*, 13(2), 292–309. https://doi.org/10.1175/1520-

- 641 0485(1983)013<0292:tvt>2.0.co;2
- Ma, X., Jing, Z., Chang, P. Liu, X., Montuoro, R., Small, R. J., Bryan, F. O., Greatbatch,
- R. J., Brandt, P., Wu, D., Lin, X., and Wu, L. (2016). Western boundary currents
- regulated by interaction between ocean eddies and the atmosphere. *Nature*, 535,
- 533–537. https://doi.org/10.1038/nature18640
- McCreary, J. P. Jr., and Lu, P. (1994). Interaction between the subtropical and equatorial
- ocean circulations: The subtropical cell. *Journal of Physical Oceanography*, 24(2),
- 648 466–497. https://doi.org/10.1175/1520-0485(1994)024<0466:IBTSAE>2.0.CO;2
- Moore, J. K., Fu, W., Primeau, F., Britten, G. L., Lindsay, K., Long, M., Doney, S. C.,
- Mahowald, N., Hoffman, F., and Randerson, J. T. (2018). Sustained climate
- warming drives declining marine biological productivity. Science, 359(6380),
- 652 1139–1143. https://doi.org/10.1126/science.aao6379
- Morrison, A. K., Waugh, D. W., Hogg, A. M., Jones, D. C., and Abernathey, R. P. (2022).
- Ventilation of the Southern Ocean Pycnocline. *Annual Review of Marine Science*,
- 655 14, 405–430. https://doi.org/10.1146/annurev-marine-010419-011012
- 656 Munk, W. H. (1966). Abyssal recipes. Deep Sea Research and Oceanographic
- 657 Abstracts, 13(4), 707–730. <a href="https://doi.org/10.1016/0011-7471(66)90602-4">https://doi.org/10.1016/0011-7471(66)90602-4</a>
- 658 Oschlies, A., Brandt, P., Stramma, L., and Schmidtko, S. (2018). Drivers and
- mechanisms of ocean deoxygenation. *Nature Geoscience*, 11, 467–473.
- https://doi.org/10.1038/s41561-018-0152-2
- 661 O'Neill, B. C., Tebaldi, C., van Vuuren, D. P., Eyring, V., Friedlingstein, P., Hurtt, G.,
- Knutti, R., Kriegler, E., Lamarque, J.-F., Lowe, J., Meehl, G. A., Moss, R., Riahi,
- K., and Sanderson, B. M. (2016). The scenario model intercomparison project
- (ScenarioMIP) for CMIP6. Geoscientific Model Development, 9(9), 3461–3482.
- https://doi.org/10.5194/gmd-9-3461-2016
- Pichevin, L. E., Bollasina, M., Nederbragt, A. J., and Ganeshram, R. S. (2024). North
- Atlantic temperature control on deoxygenation in the northern tropical
- Pacific. *Nature Communications*, 15, 7919. https://doi.org/10.1038/s41467-024-
- 669 <u>52197-6</u>
- Polzin, K. L., Toole, J. M., Ledwell, J. R., and Schmitt, R. W. (1997). Spatial variability
- of turbulent mixing in the abyssal ocean. Science, 276(5309), 93–96.
- https://doi.org/10.1126/science.276.5309.93
- Purkey, S. G., and Johnson, G. C. (2013). Antarctic bottom water warming and
- freshening: Contributions to sea level rise, ocean freshwater budgets, and global
- heat gain. Journal of Climate, 26(16), 6105–6122. https://doi.org/10.1175/JCLI-
- 676 **D-12-00834.1**
- Redi, M. H. (1982). Oceanic isopycnal mixing by coordinate rotation. Journal of
- 678 Physical Oceanography, 12(10), 1154–1158. https://doi.org/10.1175/1520-
- 679 0485(1982)012<1154:OIMBCR>2.0.CO;2

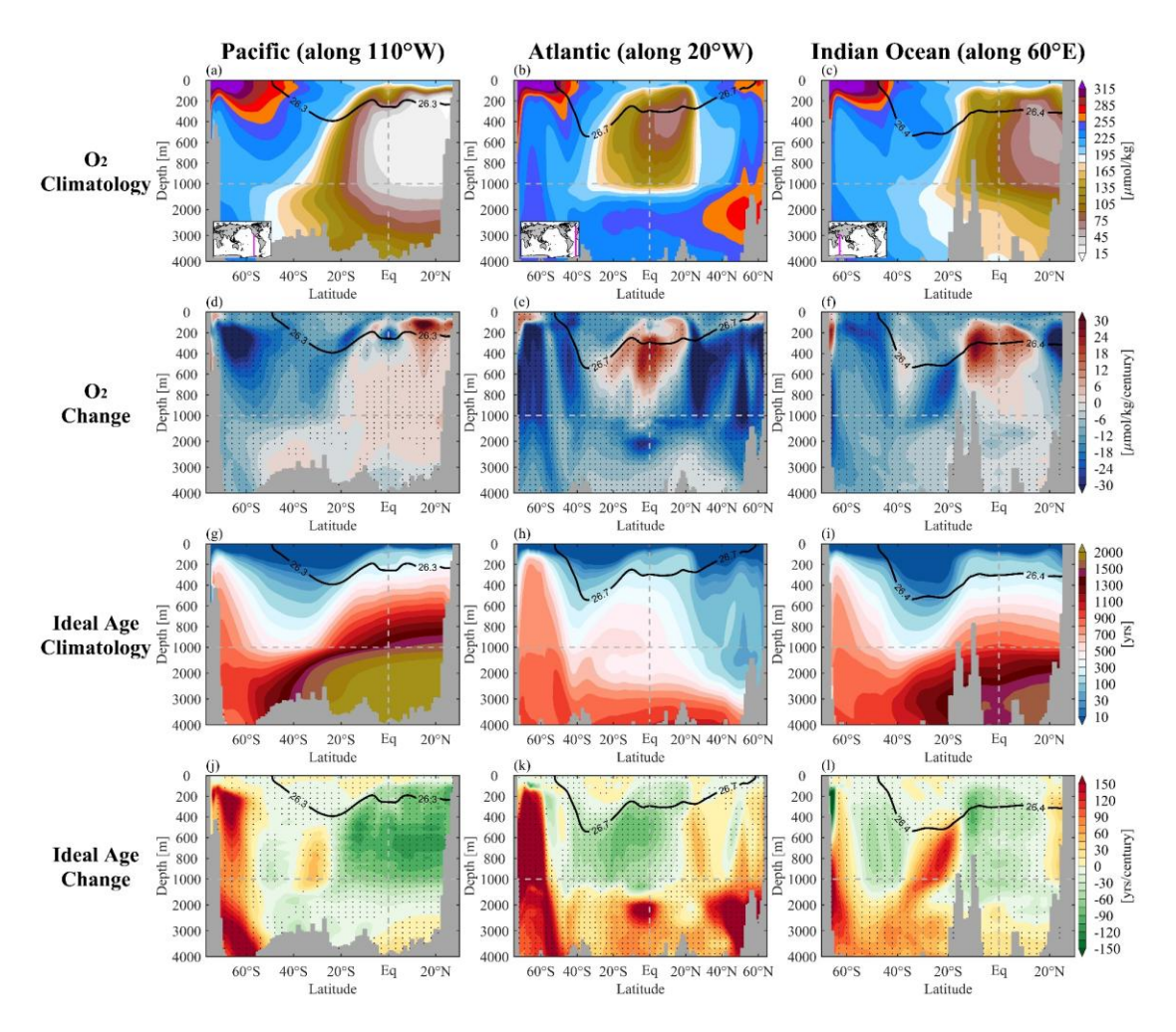
- Rohr, T., Richardson, A. J., Lenton, A., Chamberlain, M. A., and Shadwick, E. H.
- 681 (2023). Zooplankton grazing is the largest source of uncertainty for marine carbon
- 682 cycling in CMIP6 models. Communications Earth and Environment, 4, 212.
- 683 <u>https://doi.org/10.1038/s43247-023-00871-w</u>
- Ryan-Keogh, T. J., Tagliabue, A., and Thomalla, S. J. (2025). Global decline in net
- primary production underestimated by climate models. Communications Earth
- and Environment, 6, 75. https://doi.org/10.1038/s43247-025-02051-4
- 687 Schmidtko, S., Stramma, L., and Visbeck, M. (2017). Decline in global oceanic oxygen
- 688 content during the past five decades. *Nature*, 542, 335–
- 689 339. <a href="https://doi.org/10.1038/nature21399">https://doi.org/10.1038/nature21399</a>
- 690 Schmittner, A., Galbraith, E. D., Hostetler, S. W., Pedersen, T. F., and Zhang, R. (2007).
- Large fluctuations of dissolved oxygen in the Indian and Pacific oceans during
- Dansgaard-Oeschger oscillations caused by variations of North Atlantic Deep
- Water subduction. Paleoceanography and Paleoclimatology, 22(3), PA3207.
- 694 <u>https://doi.org/10.1029/2006PA001384</u>
- 695 Schmittner, A., Oschlies, A., Matthews, H. D., and Galbraith, E. D. (2008). Future
- changes in climate, ocean circulation, ecosystems, and biogeochemical cycling
- simulated for a business-as-usual CO2 emission scenario until year 4000
- 698 AD. Global Biogeochemical Cycles, 22(1), GB1013.
- 699 <u>https://doi.org/10.1029/2007GB002953</u>
- Séférian, R., Berthet, S., Yool, A., Palmiéri, J., Bopp, L., Tagliabue, A., Kwiatkowski,
- L., Aumont, O., Christian, J., Dunne, J., Gehlen, M., Ilyina, T., John, J. G., Li, H.,
- Long, M. C., Luo, J. Y., Nakano, H., Romanou, A., Schwinger, J., Stock, C.,
- Santana-Falcón, Y., Takano, Y., Tjiputra, J., Tsujino, H., Watanabe, M., Wu, T., Wu,
- F., and Yamamoto, A. (2020). Tracking improvement in simulated marine
- biogeochemistry between CMIP5 and CMIP6. Current Climate Change Reports,
- 706 6, 95–119. https://doi.org/10.1007/s40641-020-00160-0
- 707 Stocker, T. F., and Johnsen, S. J. (2003). A minimum thermodynamic model for the
- bipolar seesaw. Paleoceanography and Paleoclimatology, 18(4), 1087.
- 709 https://doi.org/10.1029/2003PA000920
- 710 Stommel, H. (1961). Thermohaline convection with two stable regimes of flow. *Tellus*,
- 711 13(2), 224–230. https://doi.org/10.1111/j.2153-3490.1961.tb00079.x
- 712 Stramma, L., Prince, E. D., Schmidtko, S., Luo, J., Hoolihan, J. P., Visbeck, M., Wallace,
- D. W. R., Brandt, P., and Körtzinger, A. (2011). Expansion of oxygen minimum
- zones may reduce available habitat for tropical pelagic fishes. *Nature Climate*
- 715 *Change*, 2(1), 33–37. https://doi.org/10.1038/nclimate1304
- 716 Sun, S., and Thompson, A. F. (2020). Centennial changes in the Indonesian
- 717 Throughflow connected to the Atlantic Meridional Overturning Circulation: The
- ocean's transient conveyor belt. Geophysical Research Letters, 47(21),
- 719 e2020GL090615. https://doi.org/10.1029/2020GL090615

- Sun, S., Thompson, A. F., and Eisenman, I. (2020). Transient overturning compensation
- 721 between Atlantic and Indo-Pacific basins. Journal of Physical
- 722 *Oceanography*, 50(8), 2151–2172. <u>https://doi.org/10.1175/JPO-D-20-0060.1</u>
- Sun, S., Thompson, A. F., Xie, S., and Long, S. (2022). Indo-Pacific warming induced
- by a weakening of the Atlantic Meridional Overturning Circulation. Journal of
- 725 *Climate*, 35(2), 815–832. https://doi.org/10.1175/JCLI-D-21-0346.1
- Sun, S., Thompson, A. F., Yu, J., and Wu, L. (2024). Transient overturning changes
- 727 cause an upper-ocean nutrient decline in a warming climate. *Nature*
- 728 *Communications*, 15, 7727. https://doi.org/10.1038/s41467-024-52200-0
- 729 Takano, Y., Ito, T., and Deutsch, C. (2018). Projected centennial oxygen trends and their
- 730 attribution to distinct ocean climate forcings. Global Biogeochemical Cycles,
- 731 32(9), 1329–1349. https://doi.org/10.1029/2018GB005939
- Vaquer-Sunyer, R., and Duarte, C. M. (2008). Thresholds of hypoxia for marine
- 533 biodiversity. Proceedings of the National Academy of Sciences, 105(40), 15452–
- 734 15457. <a href="https://doi.org/10.1073/pnas.0803833105">https://doi.org/10.1073/pnas.0803833105</a>
- 735 Xu, L., Xie, S.-P., and Liu, Q. (2012). Mode water ventilation and subtropical
- countercurrent over the North Pacific in CMIP5 simulations and future projections.
- 737 Journal of Geophysical Research: Oceans, 117(C2), C12009.
- 738 https://doi.org/10.1029/2012JC008377
- 739 Weijer, W., Cheng, W., Garuba, O. A., Hu, A. and Nadiga, B. T. (2020). CMIP6 models
- 740 predict significant 21st century decline of the Atlantic Meridional Overturning
- 741 Circulation. Geophysical Research Letters, 47(12), e2019GL086075.
- 742 https://doi.org/10.1029/2019GL086075

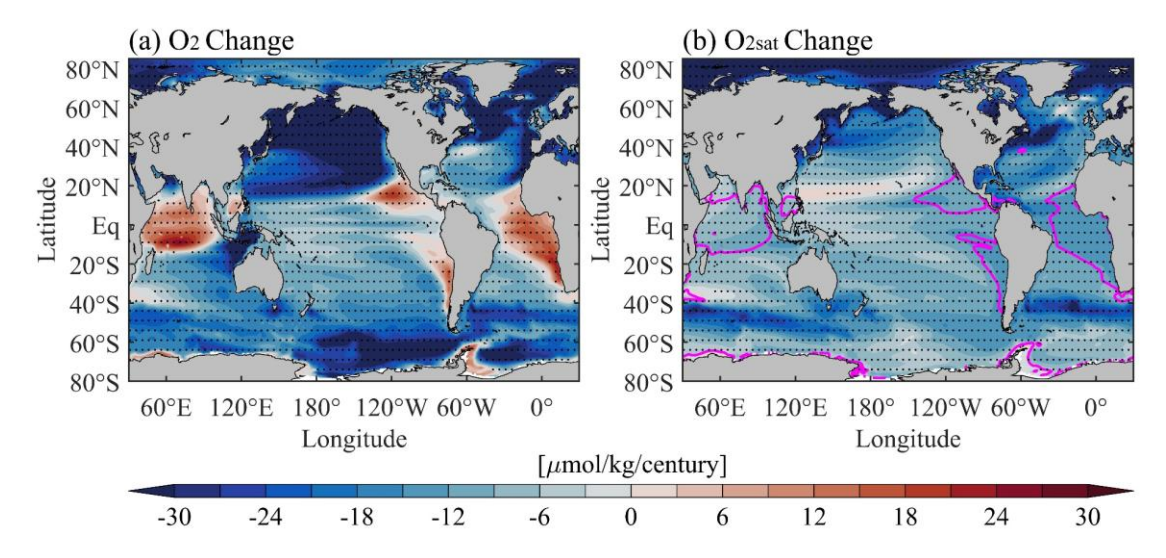
1	Supplementary material for "Extratropical forcing of low-latitude subsurface
2	oxygenation under future warming"
3	Zhen Gao <sup>1,2</sup> , Shantong Sun <sup>2,1*</sup> , Daoxun Sun <sup>2</sup> , Jimin Yu <sup>2</sup> , and Lixin Wu <sup>2</sup>
4	<sup>1</sup> College of Oceanic and Atmospheric Science, Ocean University of China, Qingdao, China
5	<sup>2</sup> Laoshan Laboratory, Qingdao, China
6	Corresponding author: Shantong Sun (stsun@qnlm.ac)
7	



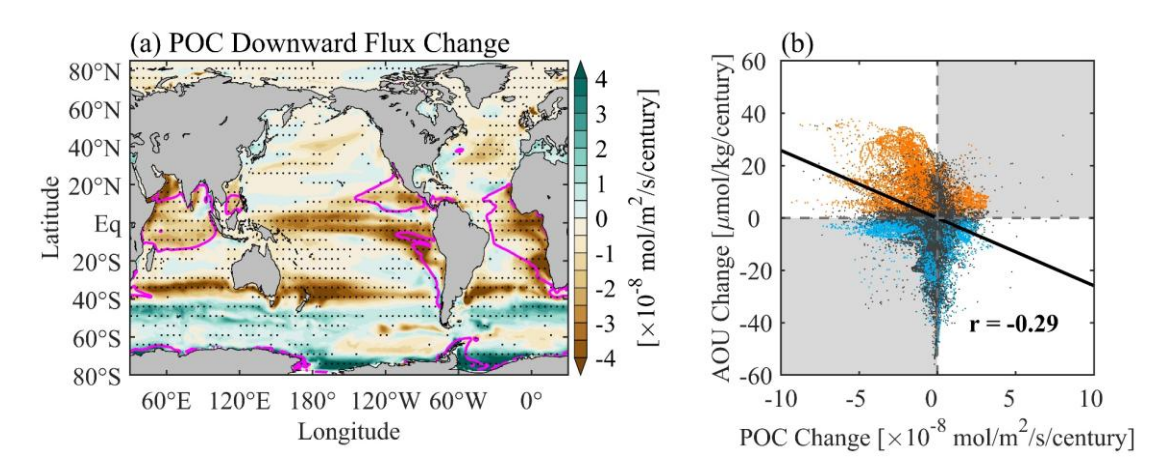
Supplementary Figure S1. Multi-model ensemble-mean vertical profiles of oxygen trends in tropical (a) Pacific, (b) Atlantic, and (c) Indian Ocean in CMIP6. Shadings represent standard deviation across CMIP6 models. The horizontal magenta lines mark 100 m and 500 m depths. Oxygen trends are averaged horizontally over regions marked by green boxes in the inset (a reproduction of Fig. 1a) to panel (c), spanning 20 degrees in longitude and 10 degrees in latitude. These regions show the most pronounced increase in subsurface oxygen concentrations in CMIP6 models.



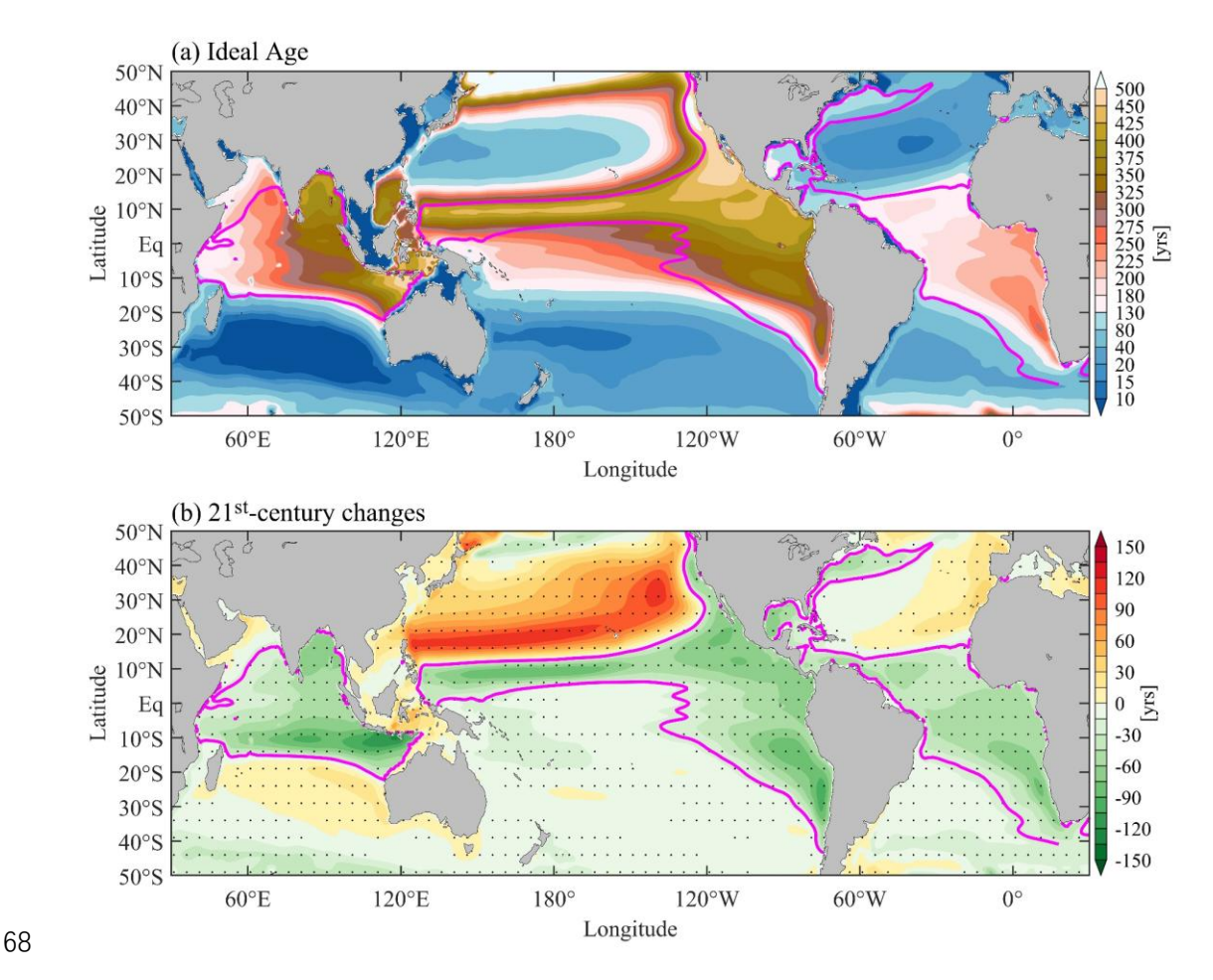
Supplementary Figure S2. Multi-model ensemble-mean oxygen and ideal age and their changes over the 21<sup>st</sup> century in CMIP6 models along (left) 110°W, (middle) 20°W, and (right) 60°E. Regions where more than 75% of models agree on the sign of changes are stippled in panels (d–f) and (j–l). Climatology values are calculated over 2015–2019 and changes are calculated based on linear trends over 2015–2100. The black contours show the depth of a specific isopycnal in each basin that approximately tracks the thermocline in mid-latitudes.



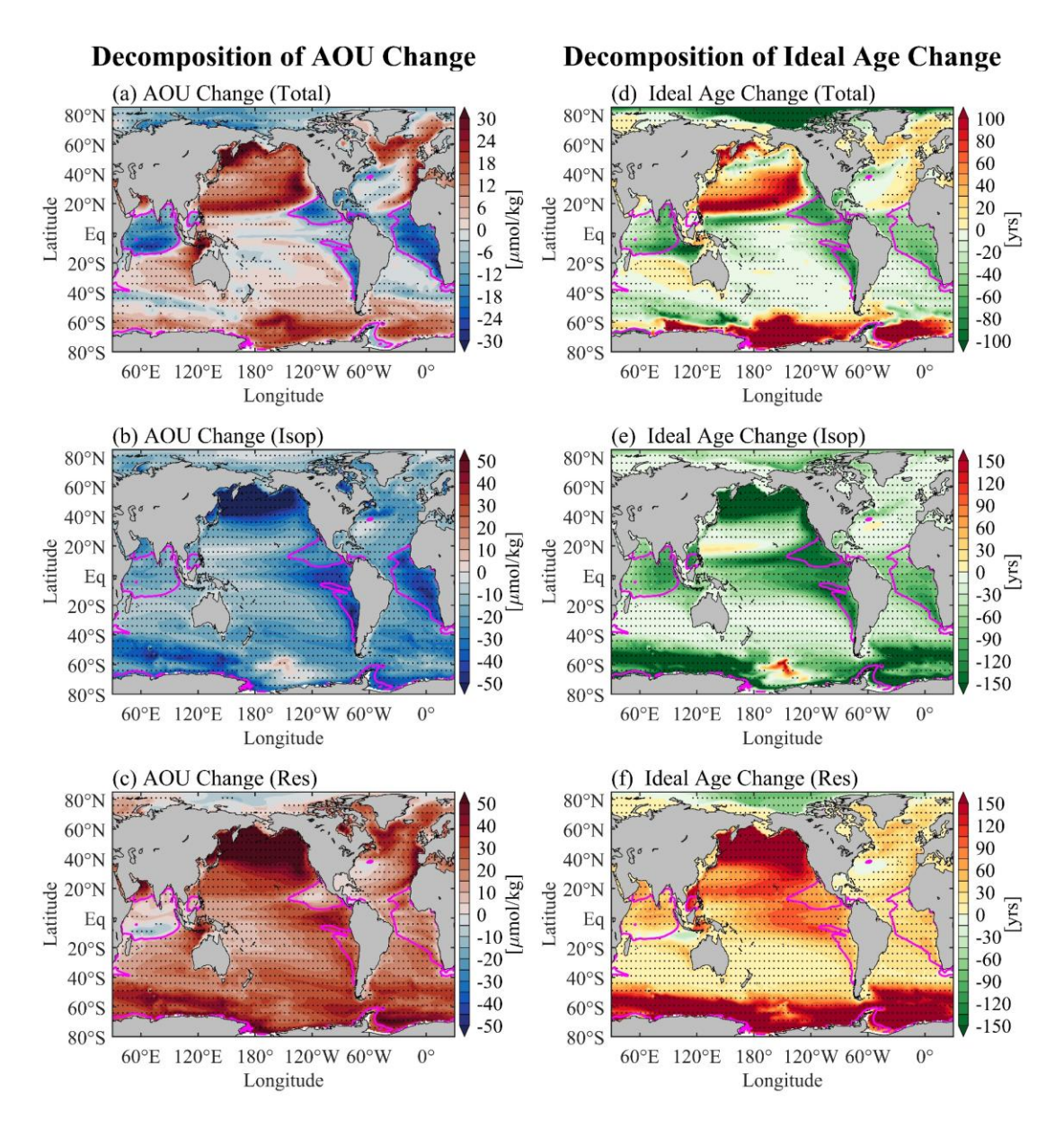
**Supplementary Figure S3. Multi-Model ensemble-mean changes in (a) oxygen concentrations** and **(b) saturated oxygen concentrations** over the 21<sup>st</sup> century, projected by CMIP6 models. Changes are calculated as linear trends from 2015 to 2100, averaged vertically over 100–500 m depths. Regions are stippled where over 75% of the models agree on the sign of changes. The magenta solid contours in (b) mark the regions where oxygen increases.



Supplementary Figure S4. Change in organic matter exporting to the subsurface and its relationship to AOU changes. (a) Linear trends of multi-model ensemble-mean downward flux of particulate organic carbon (POC) at 100 m depth over the  $21^{\rm st}$  century in CMIP6 models. Regions are stippled where over 75% of the models agree on the sign of changes. (b) Scatter plot of multi-model mean AOU changes vs. POC flux changes. The black straight line is a linear regression, with a correlation coefficient r = -0.29. Each scatter point represents a grid box of  $1^{\circ} \times 1^{\circ}$  in (a). Dots in blue and orange mean that over 75% of the examined models agree on the sign of changes, with orange color for AOU increases and blue color for AOU decreases. Grey dots mean that less than 75% of the examined models agree on the sign of changes.

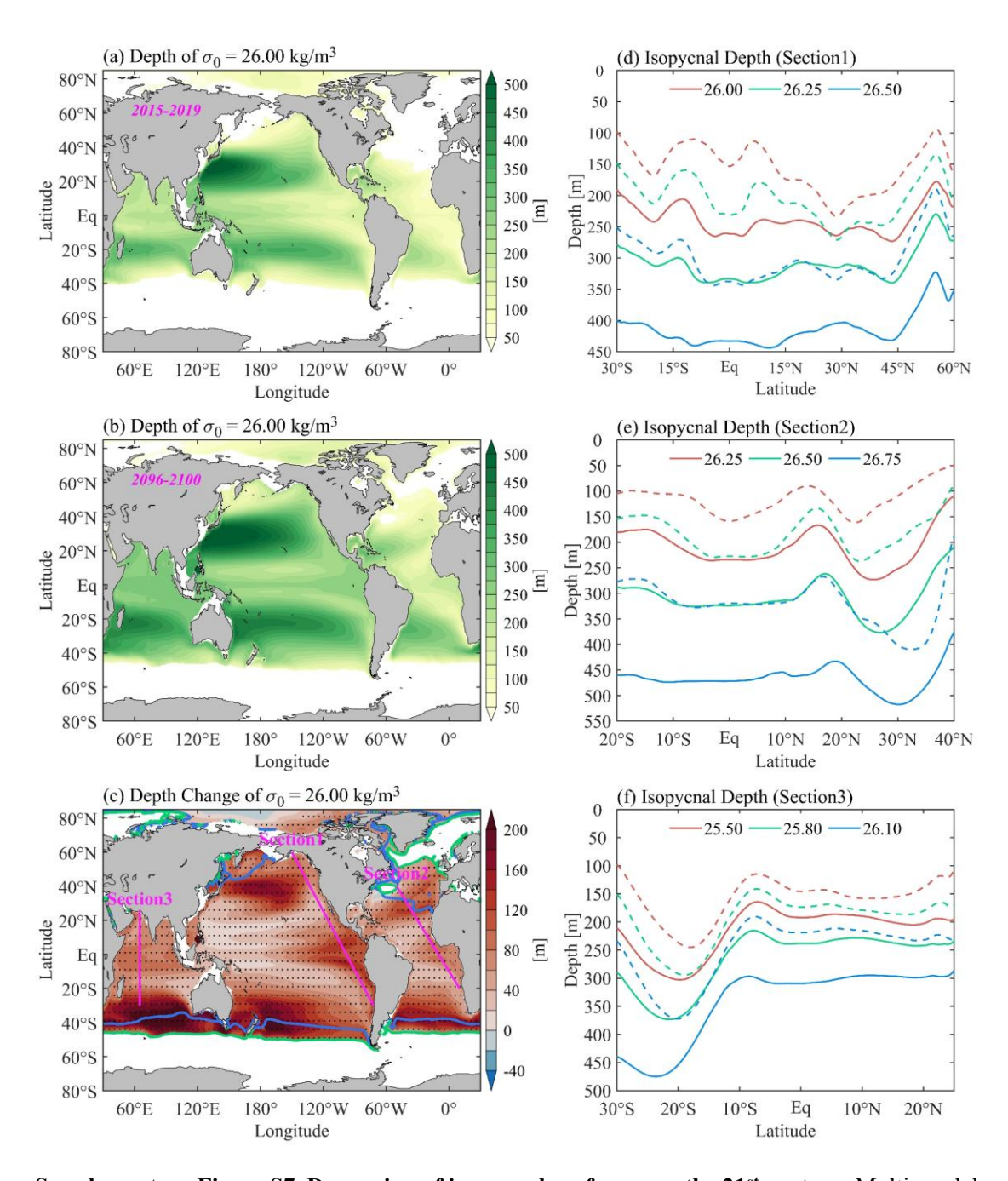


Supplementary Figure S5. Subsurface seawater ideal age and its 21<sup>st</sup>-century changes in CMIP6. (a) Seawater ideal age averaged vertically over 100–500 m and in time over 2015–2019. (b) 21<sup>st</sup>-century changes of seawater ideal age, averaged between 100–500 m and calculated as differences between 2096–2100 and 2015–2019. The magenta contour of -20 years in (b) marks the region of enhanced ventilation in low latitudes, which is occupied by relatively old water at present (a).

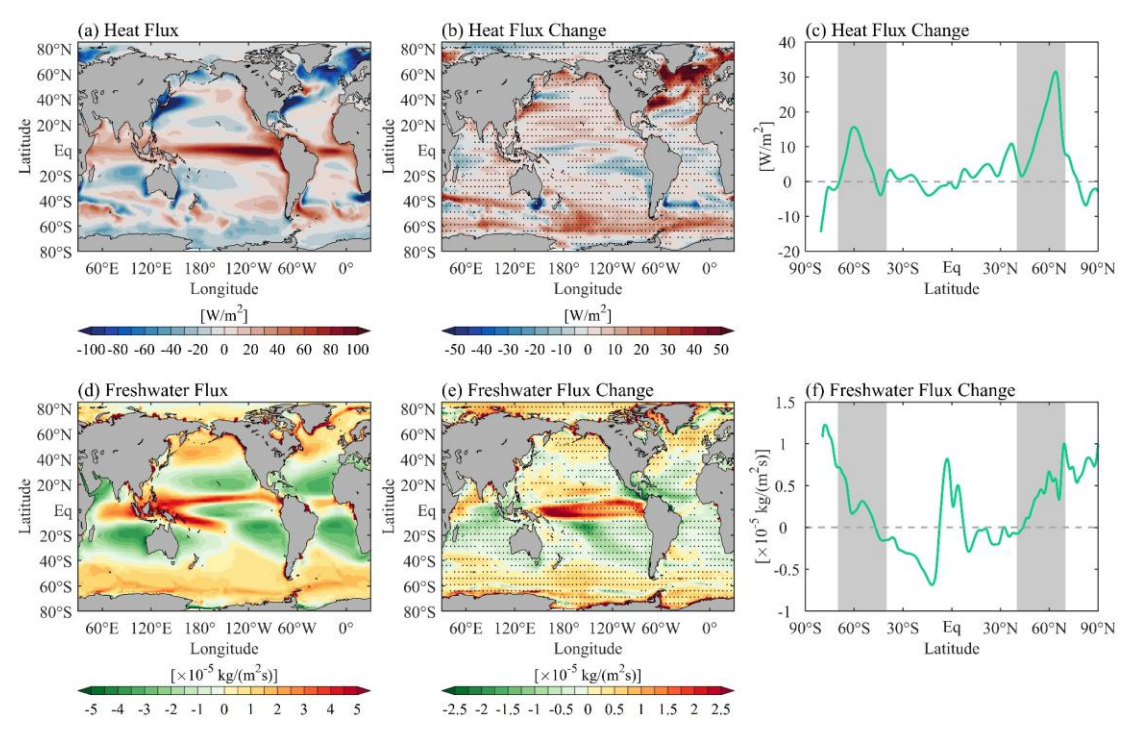


Supplementary Figure S6. Decomposition of changes in AOU and ideal age in CMIP6. (a)

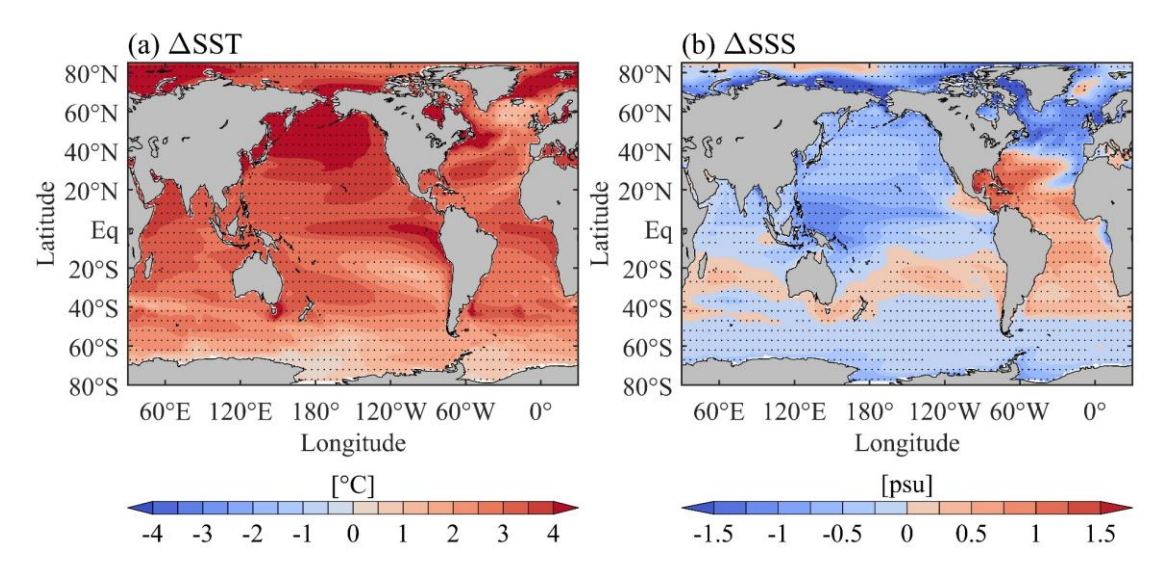
Multi-model ensemble-mean changes in *AOU*, averaged vertically between 100–500 m depths, over the 21<sup>st</sup> century. *AOU* changes due to (b) vertical movements of isopycnal surfaces and (c) other processes (see "Decomposition of AOU and idea age" in Methods). *AOU* changes due to other processes are calculated as the residual between (a) and (b). (d) Multi-model ensemble-mean ideal age changes, averaged vertically between 100–500 m depths, over the 21<sup>st</sup> century. Idea age changes due to (e) vertical movements of isopycnal surfaces and (f) other processes. Regions are stippled where over 75% of the models agree on the sign of changes. The magenta contour indicates regions where subsurface oxygen increases. Panel (e) is the same as Figure 2a in the main article.



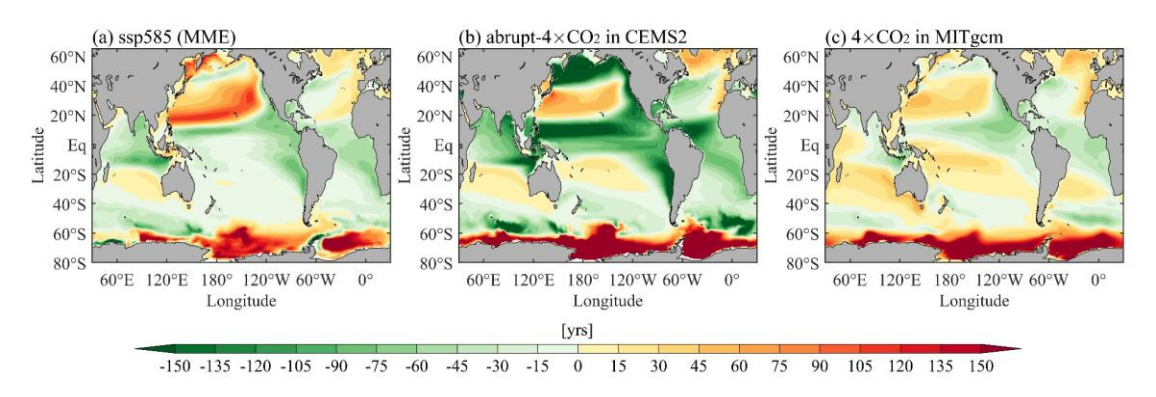
Supplementary Figure S7. Deepening of isopycnal surface over the 21<sup>st</sup> century. Multi-model ensemble-mean depth of  $\sigma_0 = 26.00 \text{ kg/m}^3$  during (a) 2015–2019 and (b) 2096–2100. (c) Depth changes of  $\sigma_0 = 26.00 \text{ kg/m}^3$  over the 21<sup>st</sup> century, calculated as the difference between (a) and (b). Regions are stippled where over 75% of the models agree on the sign of changes. (d–f) Depths of three selected isopycnals along sections indicated in panel (c). Dashed lines represent isopycnal depth averaged over 2015–2019 and solid lines denote isopycnal depths averaged over 2096–2100. Panel (c) is the same as Figure 2b in the main article.



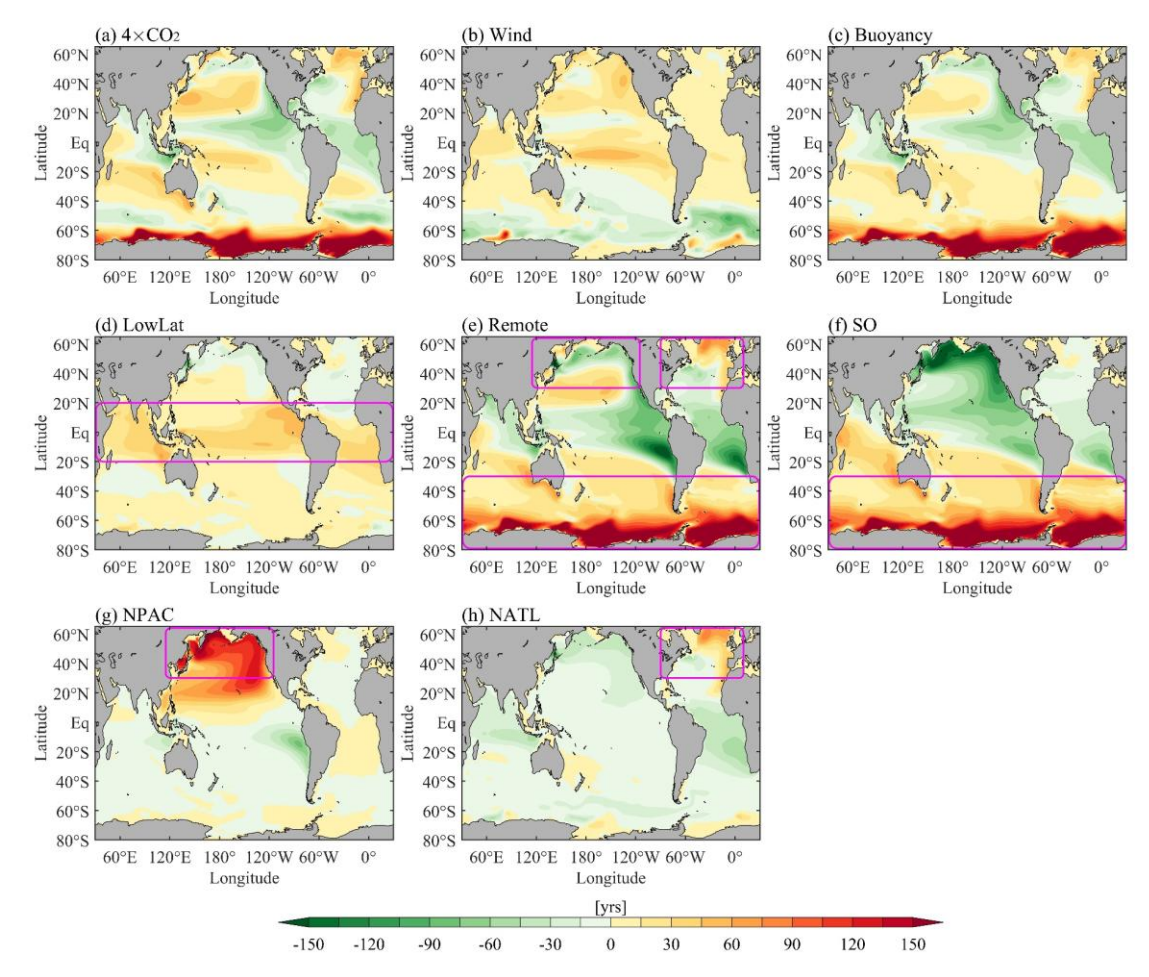
**Supplementary Figure S8.** Surface heat and freshwater fluxes in CMIP6. Multi-model ensemble-mean surface (a) net heat flux and (d) freshwater flux, averaged over 2015–2019. Changes in surface (b) net heat flux and (e) freshwater flux over the 21<sup>st</sup> century. Areas are stippled where over 75% of the models agree on the sign of changes. Zonal-mean surface (c) heat and (f) freshwater fluxes over the 21<sup>st</sup> century. Shading highlights the extratropical regions with increased heat or freshwater fluxes into the ocean. Positive values for heat and freshwater fluxes are into the ocean.



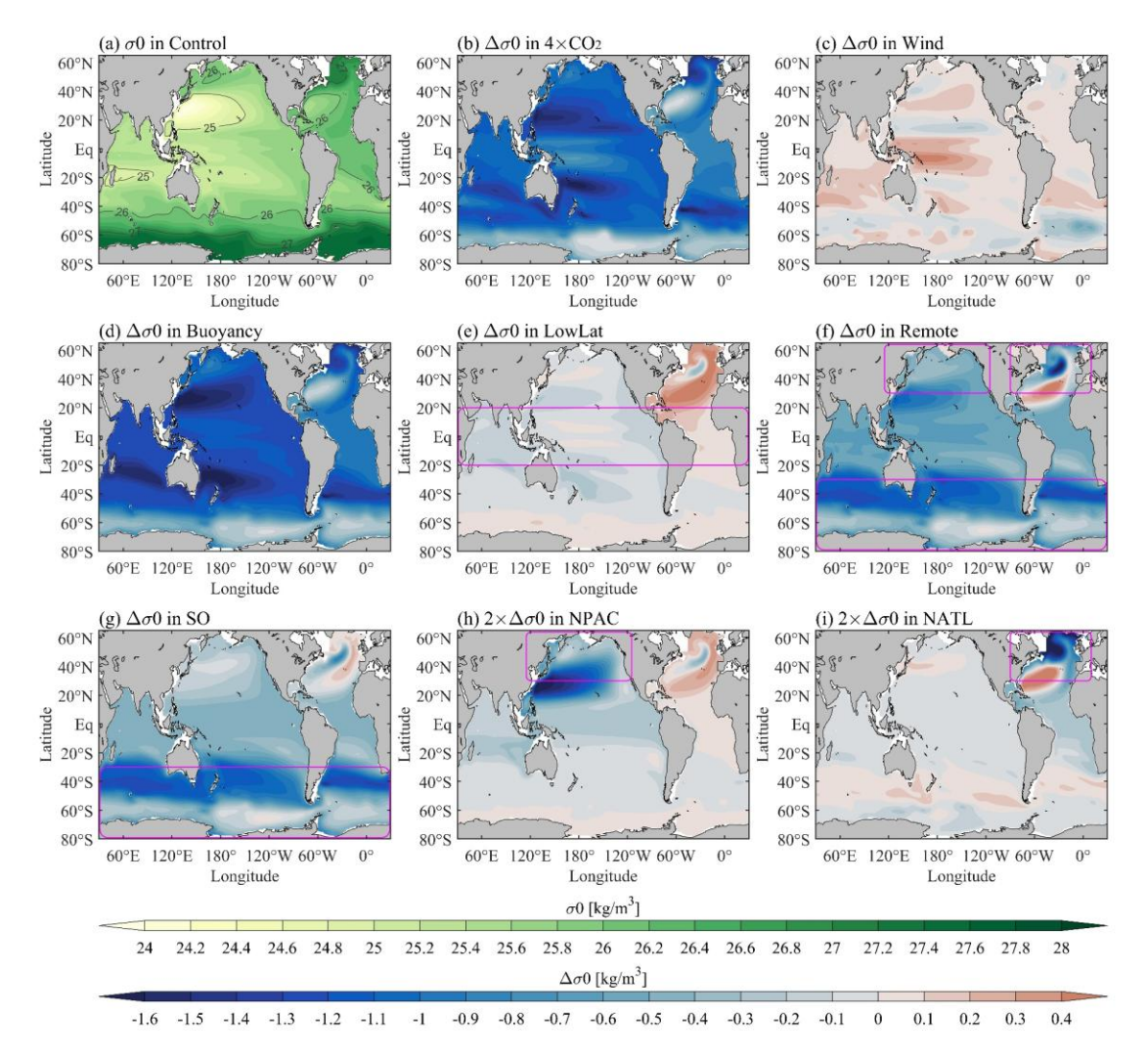
**Supplementary Figure S9.** Sea surface temperature and salinity changes in CMIP6. Multimodel ensemble-mean (a) sea surface temperature and (b) sea surface salinity changes, evaluated as the difference between 2015–2019 and 2096–2100. Stippling indicates over 75% of the models agree on the sign of changes.



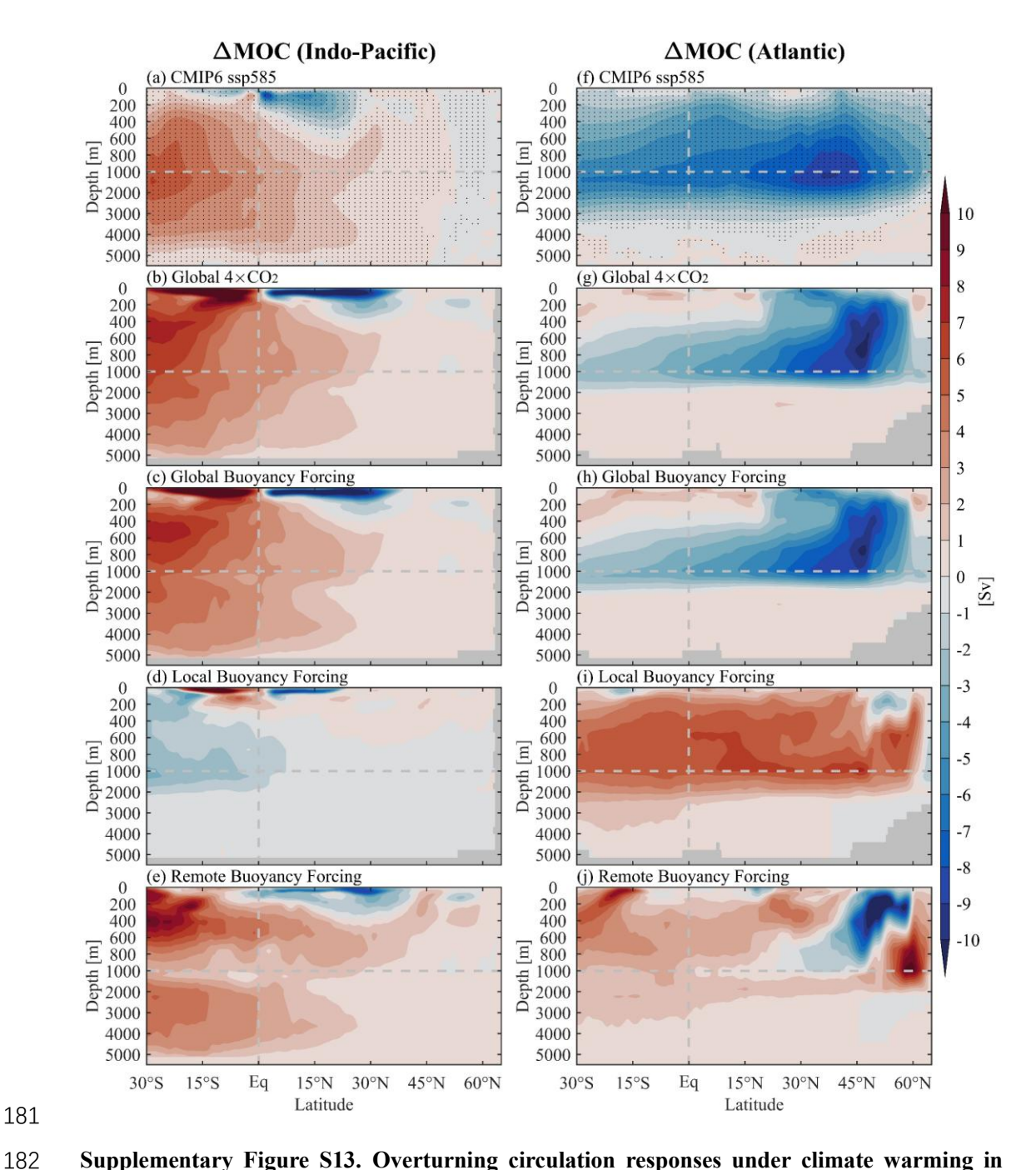
**Supplementary Figure S10.** Ventilation changes under climate warming in CMIP6, CESM2, and MITgcm. (a) Multi-model ensemble-mean ideal age changes in CMIP6, calculated as the difference between 2015–2019 and 2096–2100. (b) Ideal age changes in CESM2 abrupt-4×CO<sub>2</sub> experiment, evaluated at about 195 years after CO<sub>2</sub> quadrupling. (c) Ideal age changes in MITgcm "4×CO<sub>2</sub>", evaluated at around 100 years after applying surface forcing perturbations. The age tracer in (a–c) is vertically averaged between 100–500 m depths.



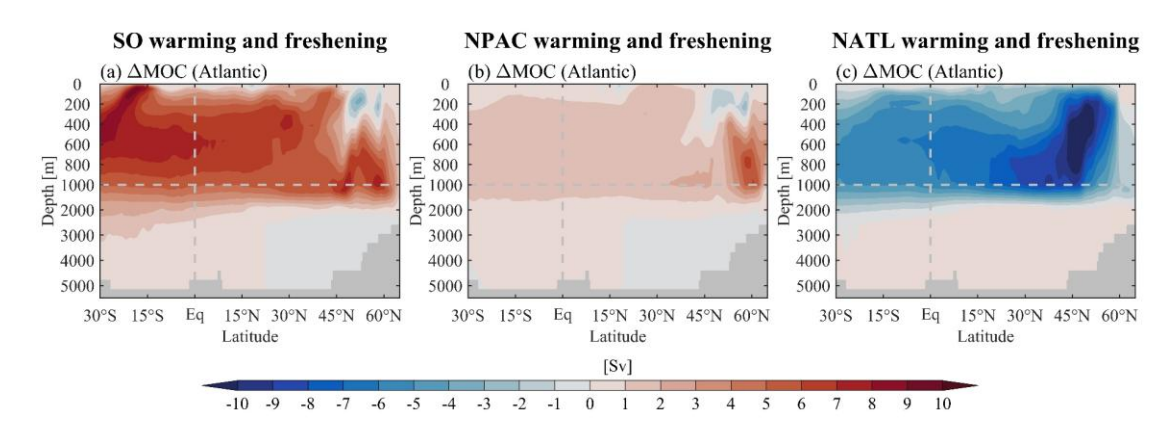
Supplementary Figure S11. Subsurface ventilation changes under forcing perturbations in MITgcm simulations (see "MITgcm simulations" in Methods). Ventilation changes, averaged vertically between 100–500 m depths, are evaluated after about 100 years of perturbations (years 95–105). The Magenta boxes in panels (d)–(h) indicate the regions where surface forcing perturbations are applied. Panels (a) and (d) are the same as Figures 3a and 3b in the main article, respectively.



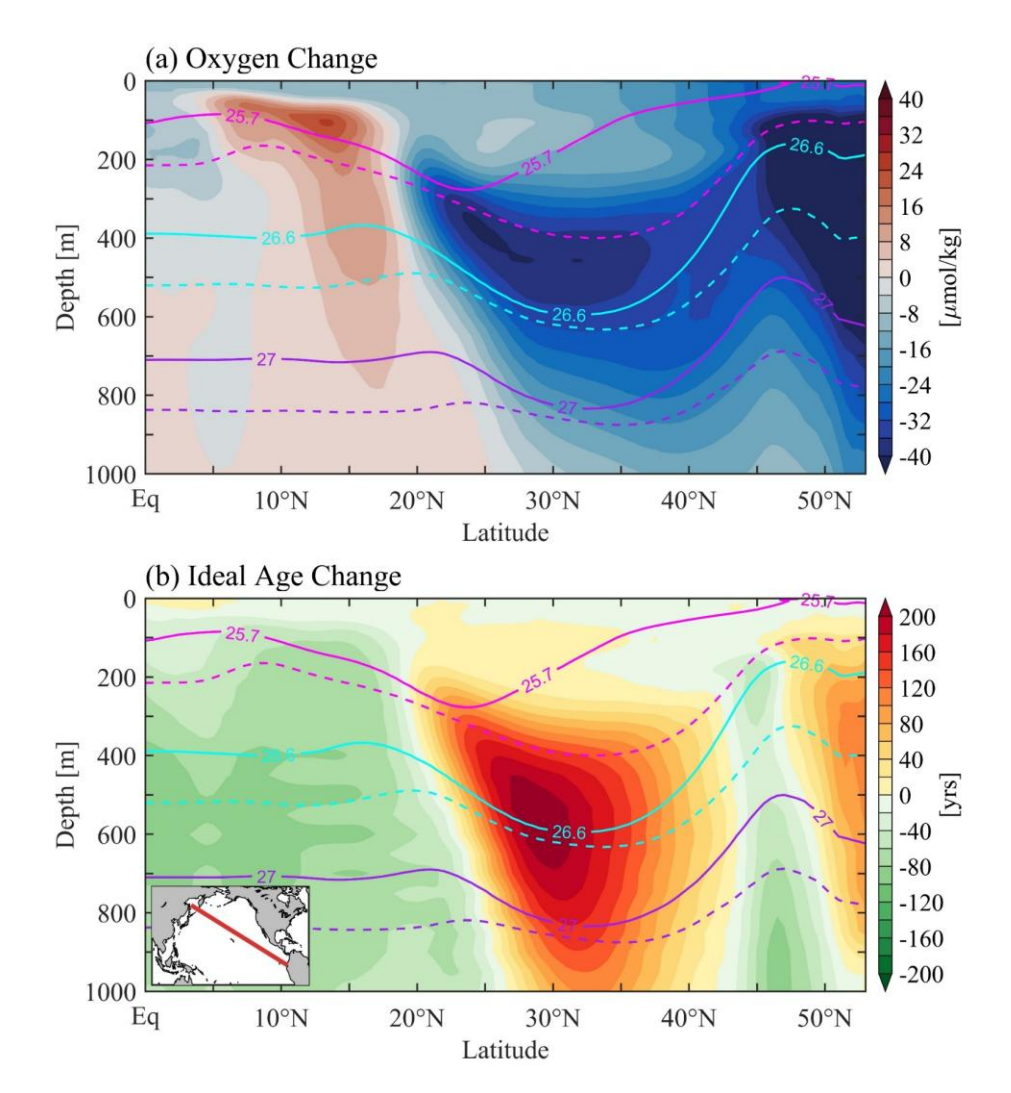
Supplementary Figure S12. Density changes under different forcing perturbations in MITgcm, averaged vertically over 100–500 m depths. (a) Potential density ( $\sigma_0$ ) distribution in Control. (b-i) Potential density changes due to forcing perturbations in (b) "4×CO2", (c) "Wind", (d) "Buoyancy", (e) "LowLat", (f) "Remote", (g) "SO", (h) "NPAC", and (i) "NATL". Positive density anomaly suggests shoaling of isopycnals and negative values suggest deepening. Notably, density changes close to the subduction regions may be driven by advections, not associated with overturning adjustments (Luongo et al., 2025). Magenta boxes in panels (d)–(h) indicate the regions where surface forcing perturbations are applied. The density anomalies in (h) and (i) are multiplied by 2 for presentation.



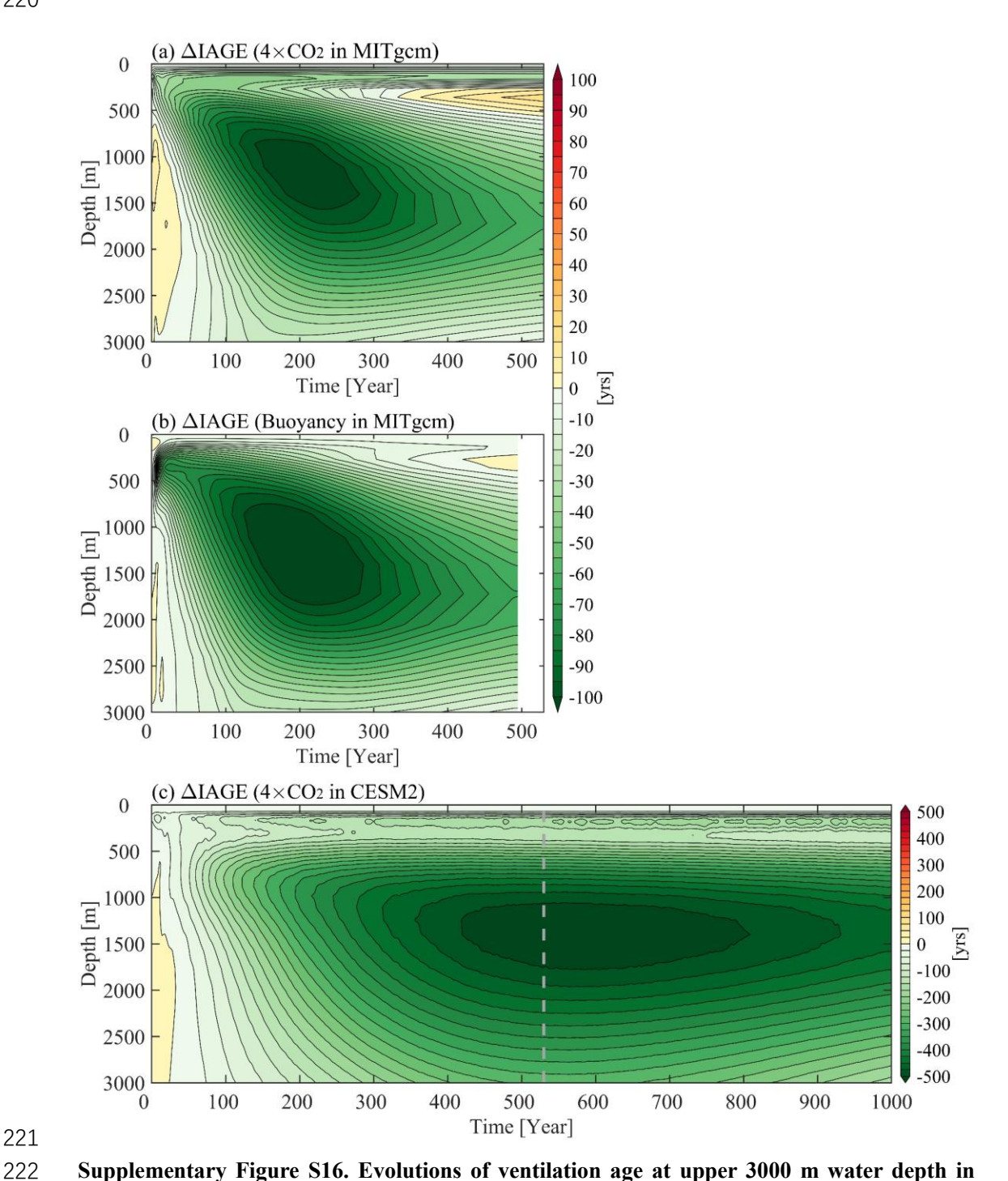
Supplementary Figure S13. Overturning circulation responses under climate warming in CMIP6 and MITgcm. Left (a—e) and right (f—j) columns show overturning circulation changes in Indo-Pacific and Atlantic, respectively. Stippling in (a) and (f) indicates over 75% of the models agree on the sign of changes. Positive and negative values for clockwise and anticlockwise overturning circulation anomalies, respectively.



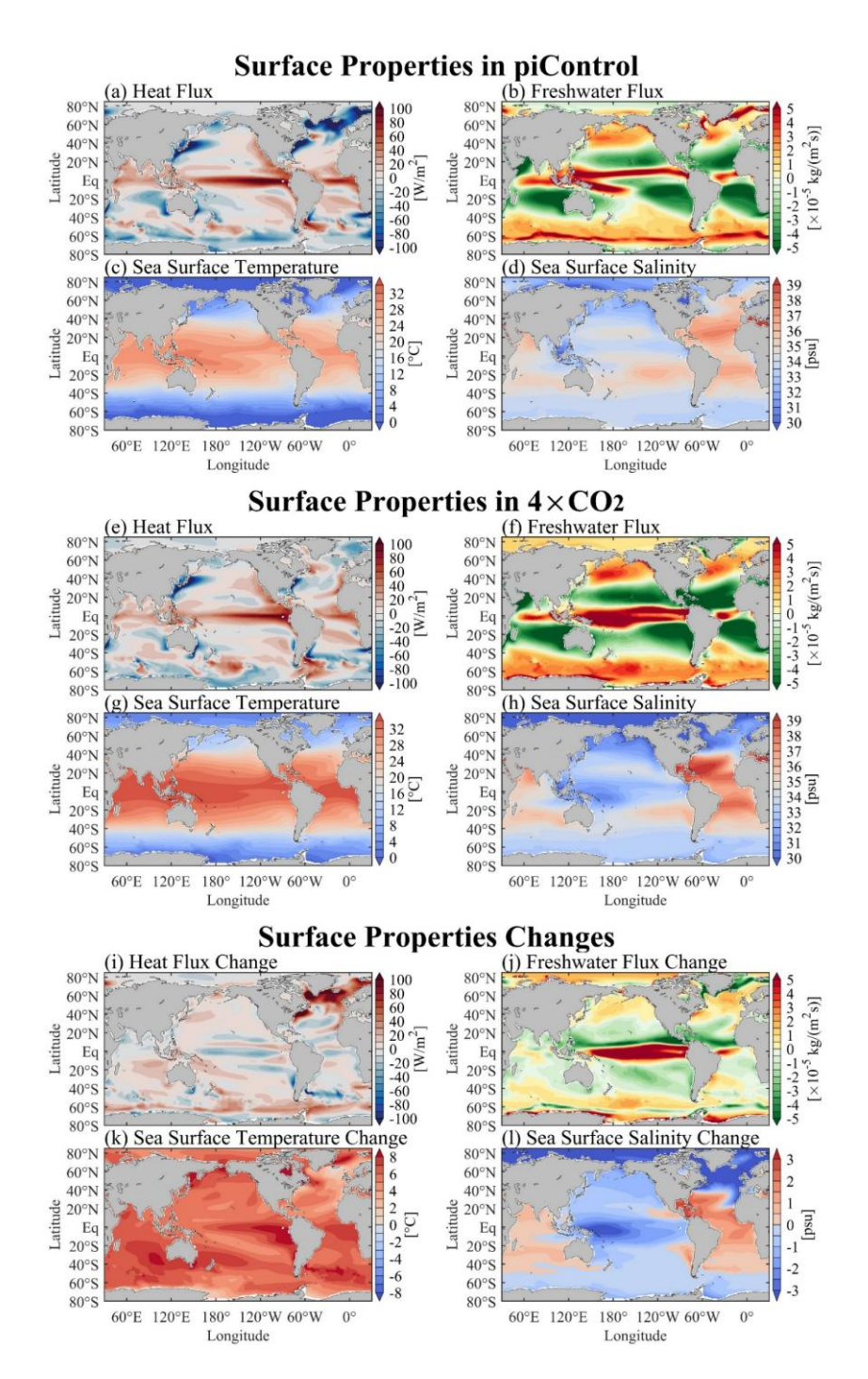
**Supplementary Figure S14. Atlantic overturning responses under extratropical warming and freshening in MITgcm.** Positive and negative values for clockwise and anticlockwise overturning anomalies, respectively. Changes are evaluated after about 100 years (years 95–105) of perturbations.



Supplementary Figure S15. CMIP6 model evidence for extratropical forcing of oxygen and ventilation changes schematized in Fig. 4. Projected multi-model mean changes (2096-2100 minus 2015-2019) in (a) oxygen concentration and (b) ideal age. The data are shown for the upper 1000 m along a transect crossing the North Pacific (inset, panel b). Three isopycnals ( $\sigma_0 = 25.7 \text{ kg/m}^3$ , magenta;  $\sigma_0 = 26.6 \text{ kg/m}^3$ , cyan; and  $\sigma_0 = 27.0 \text{ kg/m}^3$ , purple) are shown as solid and dashed contours, with solid contours for years 2015–2019 and dashed contours for years 2096–2100. The observed dipole – oxygen decrease and ventilation age increase in the subtropics contrast with oxygen increase and ventilation age decrease in the tropical subsurface – directly supports the mechanism proposed in Fig 4: extratropical changes lead to reduced subtropical subduction but enhanced tropical ventilation via isopycnal deepening.



Supplementary Figure S16. Evolutions of ventilation age at upper 3000 m water depth in MITgcm experiments and abrupt-4×CO<sub>2</sub> of CESM2. The ideal age is averaged horizontally within 230–250°E and 10–20°N. The grey dashed line in panel (c) represents 530th year, corresponding to the last year of the MITgcm experiment.



**Supplementary Figure S17. Surface properties and their changes in 4×CO<sub>2</sub> of CESM2, used to force the MITgcm simulations.** (a)–(d) Surface properties in piControl of CESM2, averaged over the last 50 years of piControl. (e)–(h) Surface properties in 4×CO<sub>2</sub> of CESM2, averaged over years 150–200. (i)–(l) Surface properties changes, evaluated as the difference between years 150–200 of 4×CO<sub>2</sub> and the last 50 years of piControl. Positive values for heat and freshwater fluxes are into the ocean.

# Supplementary Tabel S1. CMIP6 models analyzed in this study

Model	Member	Model	Member
ACCESS-ESM1-5	rlilp1f1	KIOST-ESM	rlilplfl
CanESM5	rlilp1f1	MIROC-ES2H	rlilp4f2
CanESM5-1	rlilplfl	MIROC-ES2L	rlilp1f2
CanESM5-CanOE	rlilp2f1	MPI-ESM1-2-HR	rlilplfl
CESM2	r4i1p1f1	MPI-ESM1-2-LR	rlilplfl
CMCC-ESM2	rlilp1f1	MRI-ESM2-0	rli2p1f1
CNRM-ESM2-1	rlilp1f2	NorESM2-LM	rlilplfl
GFDL-CM4	rlilp1f1	NorESM2-MM	rlilplfl
GFDL-ESM4	rlilp1f1	UKESM1-0-LL	rlilp1f2
IPSL-CM6A-LR	rlilplfl		